



# Two-Dimensional Nanomaterials With Enzyme-Like Properties for Biomedical Applications

Shuangfei Cai<sup>1</sup> and Rong Yang<sup>1,2\*</sup>

<sup>1</sup> Chinese Academy of Sciences Key Laboratory for Biomedical Effects of Nanomaterials and Nanosafety, Center of Materials Science and Optoelectronics Engineering, Chinese Academy of Sciences Center for Excellence in Nanoscience, National Center for Nanoscience and Technology, University of Chinese Academy of Sciences, Beijing, China, <sup>2</sup> Sino-Danish Center for Education and Research, Sino-Danish College, University of Chinese Academy of Sciences, Beijing, China

Recently, remarkable progress has been made in nanozyme research due to the rapid development of nanomaterials. Two-dimensional nanomaterials such as metal nanosheets, graphene-based materials, transition metal oxides/dichalcogenides, etc., provide enhanced physical and chemical functionality owing to their ultrathin structures, high surface-to-volume ratios, and surface charges. They have also been found to have high catalytic activities in terms of natural enzymes such as peroxidase, oxidase, catalase, and superoxide dismutase. This review provides an overview of the recent progress of nanozymes based on two-dimensional nanomaterials, with an emphasis on their synthetic strategies, hybridization, catalytic properties, and biomedical applications. Finally, the future challenges and prospects for this research are discussed.

**Keywords:** two-dimensional, nanomaterials, nanozyme, catalysis, biomedical

## INTRODUCTION

Enzymes are catalysts that speed up almost all biochemical reactions in cells. They have some inherent defects that make them unfavorable in large-scale applications. Since the fascinating discovery of enzymatically active Fe<sub>3</sub>O<sub>4</sub> nanoparticles (NPs) for immunoassay (Gao et al., 2007), the last decade has witnessed great advances in nanozyme research (Wei and Wang, 2013; Huang et al., 2019; Jiang D. W. et al., 2019), deriving from the growth of nanoscience and developments in technology. Various types of catalytic nanomaterials (NMs), primarily zero-dimensional (0D) NPs based on metals [e.g., Pt (Ju and Kim, 2015)], bimetallic compounds [e.g., AuPt (He et al., 2010)], metal oxides [e.g., Co<sub>3</sub>O<sub>4</sub> (Mu et al., 2013)], and metal chalcogenides [e.g., CuS (He et al., 2012)], have been extensively explored to mimic peroxidases (PODs), oxidases (ODs), catalases (CATs), and superoxide dismutases (SODs) for biomedical applications. Despite much progress in the structural design of 0D nanozymes, there are still several obvious drawbacks. Firstly, most metal-based NPs are often used in a disposable manner, which inevitably causes either economic concerns for the precious metals used or environmental issues due to the pollution and toxicity of these heavy metals (Zhang T. et al., 2014). Secondly, it is known that NPs tend to agglomerate because of huge surface energy, which decreases catalytically active sites, impairing catalytic performance (Yang et al., 2004). Lastly, the inherently imperfect surface accessibility of 0D nanostructures is unfavorable and it is difficult to fully exert the biocatalytic capacity to mimic enzymes (Maromeze et al., 2016). Therefore, researchers should develop nanozymes with novel types of structures and functionalities, a significant research frontier in the nanozyme area.

## OPEN ACCESS

### Edited by:

Kelong Fan,  
Institute of Biophysics (CAS), China

### Reviewed by:

Sanjay Singh,  
Ahmedabad University, India  
Moon Il Kim,  
Gachon University, South Korea  
Wei Chen,  
Fujian Medical University, China

### \*Correspondence:

Rong Yang  
yangr@nanoctr.cn

### Specialty section:

This article was submitted to  
Nanoscience,  
a section of the journal  
Frontiers in Chemistry

Received: 26 May 2020

Accepted: 28 October 2020

Published: 27 November 2020

### Citation:

Cai S and Yang R (2020)  
Two-Dimensional Nanomaterials With  
Enzyme-Like Properties for Biomedical  
Applications. *Front. Chem.* 8:565940.  
doi: 10.3389/fchem.2020.565940

Two-dimensional (2D) NMs within general sheet-like structures are a newly emerging but very important class of materials. Their lateral dimensions are generally one or several orders of magnitude larger than the thickness, with typical morphologies of nanosheets (NSs), nanoribbons, nanoplates, and nanowalls (Zhang, 2015). Different from their 0D counterparts, 2D NMs with these unique shapes could render large specific surface and distinctive physicochemical attributes, especially in terms of extraordinary surface chemistry, due to the exposure of most of the atoms in 2D NMs on their surface. Initial work about layered materials focused on MoS<sub>2</sub>, dating back nearly half a century (Gan et al., 2017). A surge of interest and studies on 2D NMs started after the discovery of graphene in 2004 (Novoselov et al., 2004). Since then, a host of 2D NMs, including layered double hydroxides (LDHs) (Harvey et al., 2016), transition metal dichalcogenides (TMDs) (Zhu et al., 2013), ultrathin metal NMs (Huang et al., 2011), transition metal oxides (TMOs) (Zhou et al., 2017), Xenes (e.g., black phosphorus) (Khan et al., 2020), metal carbides/nitrides (MXenes) (Jiang C. M. et al., 2019), graphitic carbon nitride (*g*-C<sub>3</sub>N<sub>4</sub>) (Yang et al., 2013), hexagonal boron nitride (*h*-BN) (Chen M. M. et al., 2017), and metal-organic frameworks (MOFs) (Ding et al., 2017), have attracted considerable attention in numerous research fields, such as sensing, catalysis/electrocatalysis, batteries, electronics/optoelectronics, supercapacitors, and biomedical areas.

In terms of mechanical, chemical, and optical attributes, the potential biocompatibility and degradability, 2D NMs have been enthusiastically researched in various biomedical fields including biosensing (Oudeng et al., 2018), antibacterial agents (Lu et al., 2017), bioimaging (Ma D. T. et al., 2020), and cancer therapy (Kong et al., 2017). Also, with a single-atom layer or several-atoms-thick layers, 2D NMs possess the highest specific surface areas among all known materials, thus they have large reservoirs and abundant anchoring sites to load and deliver therapeutic agents (Qian et al., 2017). Moreover, the planar structure endows them with unusual properties including light/ultrasonic/magnetic responses and biological behaviors (e.g., endocytosis, biodistribution, biodegradation, and excretory pathways), which evokes the broad interest in developing 2D NMs as biomaterials (Chimene et al., 2015).

The rapid development of 2D NMs as versatile biomaterials has benefited from significant research progress in graphene, especially its bulk-quantity production and surface functionalization to improve its water solubility (Li et al., 2008; Sun et al., 2008), which paved the way for graphene to be potentially utilized for biomedical purposes. Meanwhile, it should be pointed out that, the success of 0D nanozymes in biomedical applications has promoted the exploration of the enzymatic properties of other nanostructures. As the first example of the employment of 2D NMs to mimic enzymes, the carboxyl-modified graphene oxide (GO) NSs were found to be able to mimic horseradish peroxidase (HRP), which were further developed as a glucose biosensor based on POD-like activity (Song et al., 2010). Later, a large number of 2D NMs with enzymatic activities have been successively reported and

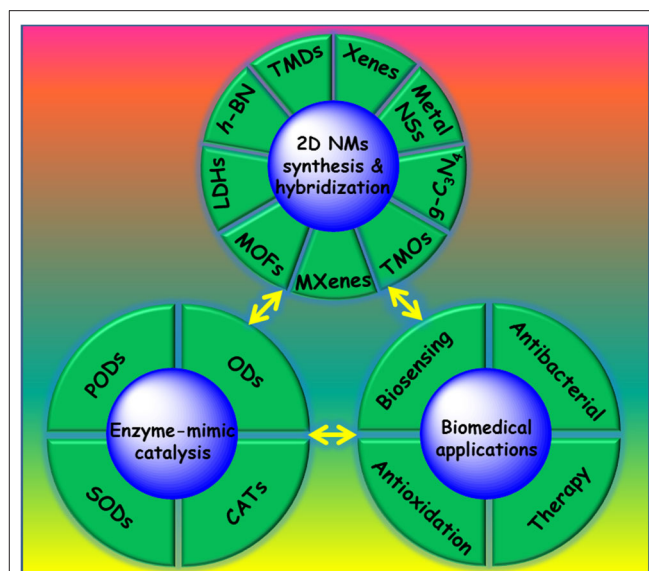


**FIGURE 1** | Two-dimensional NMs with enzyme-like activities for biomedical applications.

become a new type of enzyme-mimic, hereafter referred to as 2D nanozymes.

To our knowledge, despite many reviews (Huang et al., 2016; Agarwal and Chatterjee, 2018; Chen Y. et al., 2018; Dong et al., 2018; Merlo et al., 2018; Tao et al., 2019; Yan et al., 2019; Zhang X. L. et al., 2019; Ren et al., 2020) on the outstanding biomedical performance of 2D NMs, few of them have emphasized enzymatic properties, which are of significant importance to the development of 2D NMs. In this mini-review, we aim to highlight recent progress in 2D NMs with enzymatic properties for biomedical applications. Firstly, we briefly introduce crystal structures, synthesis, and hybridization strategies for 2D NMs. Then, we discuss the enzyme-like activities of 2D NMs. In the following, we summarize the recent advances of 2D nanozymes in diversified biomedical applications, ranging from biosensors, antibacterial agents, and antioxidants to therapeutics (Figure 1). Finally, we share our insights into the development prospects and challenges of 2D nanozymes.

## CRYSTAL STRUCTURES, SYNTHESIS, AND HYBRIDIZATION STRATEGIES OF 2D NMs

### Crystal Structures of 2D NMs

In essence, the unusual physicochemical attributes of 2D NMs largely depends on their atomic arrangements, which have been clarified in detail elsewhere (Butler et al., 2013; Zhang, 2015; Tan et al., 2017). Despite multifarious composition and structural differences, 2D NMs can be generally categorized as layered and non-layered (Hu et al., 2019). For the former, each in-plane atom connects to the neighboring ones through strong chemical bonding in every layer. The layers, however, stack together via weak van der Waals (VDW) interaction (Bhimanapati et al., 2015). A typical layered compound is graphite, in which each

atom covalently bonds to three adjacent atoms in planes by  $\sigma$ -bond but weak VDW interaction exists between layers (Allen et al., 2010). LDHs, TMDs,  $g$ - $C_3N_4$ ,  $h$ -BN, Xenes, MXenes, and MOFs, also have a graphite-like crystallite structure. By contrast, the non-layered NMs crystallize in three dimensions by atomic/chemical bonds to form bulk crystals, which typically include 2D metals, metal oxides/chalcogenides, and others (Tan and Zhang, 2015). Relying on the specific arrangement of atoms, coordination modes between atoms, or stacking order between layers, these non-layered NMs can crystallize into different crystal phases, which greatly affect their attributes and functionalities (Tan et al., 2017).

## Synthetic Approaches of 2D NMs

The top-down and bottom-up methodologies, as two types of commonly used approaches to the synthesis of 2D NMs, are well-summarized in the literature (Chen et al., 2015; Tan et al., 2017). The former is based on direct cleavage of bulk precursors, aiming to break weak VDW interaction between layers in 2D NMs by various driving forces, typically mechanical/liquid-phase/ion-intercalation and exfoliation (Zeng et al., 2011; Huo et al., 2015; Yi and Shen, 2015). Notably, these methods are only suitable for layered materials. They are relatively simple but suffer from certain disadvantages and limitations. Take synthesis of  $MoS_2$  NSs for example, mechanic exfoliation (Novoselov et al., 2005) is limited by low throughput, thereby making it unsuitable for most biomedical applications: Li-intercalation process not only requires a long time (e.g., 3 days) and high temperature (e.g., 100°C) but results in semiconducting-to-metallic phase-transition of  $MoS_2$  bulk (Yuwen et al., 2016); liquid exfoliation proposes difficulties in removing high-boiling organic solvents (Coleman et al., 2011).

Contrarily, the bottom-up methods usually begin with small organic or inorganic molecules/atoms, employing crystal growth/assembly into a 2D ordered structure, which includes classical chemical vapor deposition (CVD) (Shi et al., 2010) and wet-chemical synthesis (hydro-/solvo-thermal (Duan et al., 2014; Huang et al., 2014) and the self-assembly (Wu et al., 2015) of crystals, etc.). Since the bottom-up methods are based on the chemical reactions of certain precursors in given synthetic systems, they are more versatile than the top-down methods in enabling access to all types of 2D NMs. Despite the above protocols, it is still challenging to develop an appropriate strategy to synthesize 2D NMs with controlled and desirable structural parameters so as to satisfy the specific requirements.

## Hybridization of 2D NMs

It is known that the hybridization of 2D NMs with functionalized species is an effective strategy to extend and expand their functionalities, which could potentially make them suitable for practical applications. Numerous functionalized species (e.g., atoms, ions, molecules, polymers, and nanostructures), have been modified onto/into 2D NMs by various methods such as doping, adsorption, electrodeposition, covalent functionalization, chemical reduction, and self-assembly (Guan and Han, 2019). For example, to improve water dispersibility and the stability of pristine MXenes NSs in a physiological solution

for biomedical applications, Shi's group reported modification of  $Ti_3C_2$  NSs with soybean phospholipid by adsorption (Lin et al., 2017). The functionalized materials were found to possess enhanced permeability, stable circulation, and retention ability. In a similar study by Geng's group, titanium carbide NSs terminated with  $Al(OH)_4^-$ , obtained by intercalation of  $Ti_3AlC_2$  bulk with tetramethylammonium (TMAOH) were modified with polyethylene glycol (PEG) molecules. The functionalized NSs demonstrated excellent stability in various physiological solutions, which were further developed as promising photothermal therapeutic agents (Xuan et al., 2016).

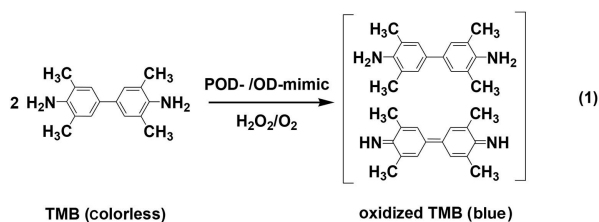
A variety of 0D metal NPs-functionalized 2D NSs have also been reported by different groups, including 0D/2D nanostructured Au/GO (Tao et al., 2013), Au/MOF (Huang et al., 2017a), and Pt/black phosphorus (Ouyang et al., 2018). In recent studies, the *in-situ* growth method was also adopted by different groups for the synthesis of Pt/ $h$ -BN (Ivanova et al., 2019) and "naked" Au NPs on  $g$ - $C_3N_4$  NSs (Wu et al., 2019), via the reduction of metal precursors on NSs with various reducing agents like  $NaBH_4$ , ascorbic acid, etc. Our group also constructed a variety of 0D/2D heterostructures, including PtAg NPs-decorated  $MoS_2$  NSs through the hydrothermal process (Cai et al., 2016), Pt NPs-covered CuO NSs by  $NaBH_4$  reduction (Wang X. H. et al., 2017), and  $IrO_2$  NPs-modified GO (Sun et al., 2020) and reduced GO (rGO) (Liu X. L. et al., 2019) NSs by electrostatic adsorption/hydrothermal treatment. The modification of NPs onto 2D NMs could not only prevent NPs from aggregation but inhibit the restacking of NSs, which could facilitate practical applications. However, to access these nanocomposites, a multi-step procedure was generally required for synthesis. In a recent study, our group reported a one-pot fabrication of PtRh NPs-modified Rh NSs (Cai et al., 2019). During the synthesis, Pt atoms/clusters as seeds were first formed by reduction of Pt precursors ( $H_2PtCl_6 \cdot 6H_2O$ ), which promoted the reduction of Rh precursors ( $Rh(acac)_3$ ) to form PtRh NPs and directed formation of Rh NSs around PtRh NPs. In another work, our group demonstrated the one-pot synthesis of Pd NPs-modified  $NiCl_2$  NSs, by using a three-step process of "*in situ* reduction-oxidation-assembly" (Cai et al., 2018a). Notably, the pre-preparation and/or functionalization of NSs as well as immobilization of NPs on NSs, generally involved in conventional synthetic protocols, were unnecessary in the above studies.

## ENZYMATIC PROPERTIES OF 2D NANOZYMES

### POD- and OD-Like Properties

PODs and ODs are a class of known oxidative enzymes in biosystems, which activate  $H_2O_2$  and  $O_2$  to catalyze the oxidation of respective substrates under mild conditions (Wei and Wang, 2013; Huang et al., 2019; Jiang D. W. et al., 2019). To evaluate the POD-/OD-like activity of 2D NMs, catalytic oxidations of enzymatic chromogenic substrates like 3,3',5,5'-tetramethylbenzidine (TMB), which are often carried out in acidic media and produce colored products (Equation 1), are

chosen as a probe reaction by most researchers (Gao et al., 2007; Song et al., 2010; Tao et al., 2013; Cai et al., 2016, 2018a, 2019; Huang et al., 2017a; Wang X. H. et al., 2017; Ouyang et al., 2018; Ivanova et al., 2019; Liu X. L. et al., 2019; Wu et al., 2019; Sun et al., 2020). The reaction process is tracked by UV-Vis spectroscopy and the color variation of the reaction solution can be easily observed by naked eyes.



Since the first report of GO NSs as a 2D POD-mimic by Qu's group (Song et al., 2010), similar observations were obtained from other types of 2D NMs, which also exhibited typical Michaelis-Menten kinetics during POD-catalysis. The apparent kinetic constant ( $K_m$ ) and maximum reaction rate ( $V_{max}$ ), as two important parameters related to enzyme-catalysis, could be determined from the Lineweaver-Burk plot. The constant  $K_m$  characterizes the binding affinity of a substrate to the enzyme, in which a lower  $K_m$  value means the higher affinity. **Table 1** lists the kinetic parameters of typical 2D NMs as POD-mimics based on GO (Zhang L. N. et al., 2014; Sun et al., 2020) or rGO (Liu X. L. et al., 2019), TMDs (Lin et al., 2014a,b; Chen T. M. et al., 2017; Huang et al., 2018; Wu et al., 2018; Feng et al., 2020), LDHs (Zhan et al., 2018; Yang et al., 2020),  $g$ - $C_3N_4$  (Darabdhara et al., 2019), MOF NSs (Chen J. Y. et al., 2018),  $h$ -BN (Ivanova et al., 2019), metal oxides (Wang X. H. et al., 2017; Li et al., 2019), and metallic NSs (Wei et al., 2015; Cai et al., 2018b, 2020).

In an earlier study on the POD-like properties of TMDs, Guo's group reported that the commercially obtained  $MoS_2$  NSs by solution-based exfoliation gave a  $K_m$  value of 0.0116 mM with  $H_2O_2$  as substrate, far lower than those of HRP (3.7 mM) (Gao et al., 2007) and  $Fe_3O_4$  NPs (154 mM) (Gao et al., 2007), suggesting good affinity of as-obtained materials toward  $H_2O_2$  (Lin et al., 2014a). The authors also found the POD-catalysis of  $MoS_2$  NSs was efficient over a broad pH range (2.0–7.5), wider than those of GO NSs and several 0D NPs [e.g.,  $Fe_3O_4$  (Gao et al., 2007),  $Co_3O_4$  (Mu et al., 2012), and  $ZnFe_2O_4$  (Su et al., 2012)]. In a recent study, Wang's group synthesized  $MoS_2$  NSs using a hydrothermal method, followed by the treatment of  $N_2$  plasma, producing N-doped  $MoS_2$  NSs (Feng et al., 2020). With  $H_2O_2$  as a substrate, the as-obtained materials not only gave a much lower  $K_m$  value (0.4459 mM) compared to that of the undoped ones (2.0828 mM), but presented a larger  $V_{max}$  value ( $4.348 \times 10^{-8} \text{ M s}^{-1}$ ) than that of undoped NSs ( $1.346 \times 10^{-8} \text{ M s}^{-1}$ ), suggesting enhanced affinity and the activity of NSs by N-doping. The  $N_2$  plasma treatment efficiently increased the surface wettability and affinity of pristine NSs, thus improving the access of the electrons and substrates of catalytic reactions. In another study, Das's group synthesized a series of metal NPs (e.g., Au, Ni, and AuNi NPs) decorated  $g$ - $C_3N_4$  NSs by a

solvothermal method (Darabdhara et al., 2019). With a substrate of either TMB or  $H_2O_2$ , the bimetallic nanocomposites gave both lower  $K_m$  values and larger  $V_{max}$  values (**Table 1**) than those of monometallic ones, indicating better affinity and POD-like activity by introducing bimetallic NPs into  $g$ - $C_3N_4$  NSs. Similar observations were obtained by Pt/CuO (Wang X. H. et al., 2017),  $IrO_2$ /rGO (Liu X. L. et al., 2019), Pd/NiCl<sub>2</sub> (Cai et al., 2018a), and PtM/ $MoS_2$  (M = Ag, Cu, and Au) (Cai et al., 2016, 2017; Qi et al., 2016) as reported by our group.

Compared to the layered NM-based POD-mimics, non-layered examples are few. In a study by our group, the Pd NSs were prepared in  $CH_3COOH$  by bubbling of CO gas, followed by Galvanic replacement of  $Au^{3+}$  ions to obtain Au NPs decorated Pd NSs (Cai et al., 2020). When TMB and  $H_2O_2$  respectively acted as a substrate, the as-obtained nanocomposites afforded two large  $V_{max}$  values ( $19.65 \times 10^{-8}$  and  $8.19 \times 10^{-8} \text{ M s}^{-1}$ ), an  $\sim 2$ -fold enhancement in those of Pd NSs ( $7.01 \times 10^{-8}$  and  $4.02 \times 10^{-8} \text{ M s}^{-1}$ ). In another study, Zheng's group synthesized ultrathin Pd NSs with a thickness below 10 atomic layers in the presence of PVP and a halide salt, followed by coating Pt nanodots onto the Pd NSs by reduction of  $Pt(acac)_2$  with hydrazine hydrate in DMF solution (Wei et al., 2015). As listed in **Table 1**, compared to Pd NSs, the as-prepared nanocomposites gave lower  $K_m$  values and larger  $V_{max}$  values, demonstrating superior affinity and activity. To further make a meaningful comparison of catalytic efficiency between Pd NSs and the nanocomposites, the catalytic rate constant ( $K_{cat}$ ) was introduced by the authors, which was calculated from the equation  $K_{cat} = V_{max}/E$ , where  $E$  is the concentration of the catalyst. With either TMB or  $H_2O_2$  as a substrate, the obtained  $K_{cat}$  value for the nanocomposites was appropriately two times larger than those of Pd NSs. However, compared to several NPs such as  $Fe_3O_4$  NPs (Gao et al., 2007), the catalytic efficiency of the nanocomposites is not high enough. In an interesting study, our group presented superior POD-catalysis of single-layer Rh NSs synthesized via the solvothermal method (Cai et al., 2018b). The obtained  $K_m$  values for Rh NSs that were comparable to those of HRP (Gao et al., 2007), while the  $V_{max}$  value for Rh with  $H_2O_2$  as the substrate was exceptionally larger than those of HRP (Gao et al., 2007), Rh NPs (Choleva et al., 2018), and layered NMs based on GO (Gao et al., 2007), and TMD-based NSs (Lin et al., 2014a,b; Chen T. M. et al., 2017; Wu et al., 2018). Moreover, the obtained  $K_{cat}$  value for Rh NSs to  $H_2O_2$  was 128 times, 323 times, and 34 times larger than those of HRP (Gao et al., 2007), Rh NPs (Choleva et al., 2018), and few-layer Pd NSs (Wei et al., 2015), respectively. This high activity could be attributed to the large number of exposed active Rh atoms that were coordinately unsaturated, which facilitated efficient interaction with reactants during catalysis. The Rh NSs also demonstrated satisfactory chemical/thermal stability.

Previous studies revealed that POD-catalysis generally involves two types of pathways: (1) the generation of reactive oxygen species (ROS) including hydroxyl radicals ( $\cdot OH$ ) (Song et al., 2010; Lin et al., 2014a; Wei et al., 2015; Wang X. H. et al., 2017; Cai et al., 2018a), and (2) electron-transfer (ET) process (Cai et al., 2018b, 2020). The former is believed to undergo a radical chain mechanism, in which the O-O bonds

**TABLE 1** | The kinetics parameters of HRP, Fe<sub>3</sub>O<sub>4</sub> NPs, and typical 2D POD-mimics<sup>a</sup>.

Catalyst	[E] (10 <sup>-12</sup> M)	Substrate	K <sub>m</sub> (mM)	V <sub>max</sub> (10 <sup>-8</sup> M S <sup>-1</sup> )	K <sub>cat</sub> (10 <sup>4</sup> s <sup>-1</sup> )	References
HRP	25	TMB	0.434	10	0.4	Gao et al., 2007
		H <sub>2</sub> O <sub>2</sub>	3.7	8.71	0.348	
Fe <sub>3</sub> O <sub>4</sub> NPs	1.14	TMB	0.098	3.44	3.02	Gao et al., 2007
		H <sub>2</sub> O <sub>2</sub>	154	9.78	8.58	
GO	NA	TMB	0.0237 ± 0.001	3.45 ± 0.31	NA	Song et al., 2010
		H <sub>2</sub> O <sub>2</sub>	3.99 ± 0.67	3.85 ± 0.22		
Pt/GO	NA	TMB	0.1864	10.2	NA	Zhang et al., 2014
		H <sub>2</sub> O <sub>2</sub>	221.4	12.45		
IrO <sub>2</sub> /GO	NA	TMB	0.56	32.8	NA	Sun et al., 2020
		H <sub>2</sub> O <sub>2</sub>	5.19	20.8		
IrO <sub>2</sub> /rGO	NA	TMB	0.276	42.7	NA	Liu X. L. et al., 2019
		H <sub>2</sub> O <sub>2</sub>	229	372.9		
MoS <sub>2</sub>	NA	TMB	0.525	5.16	NA	Lin et al., 2014a
		H <sub>2</sub> O <sub>2</sub>	0.0116	4.29		
WS <sub>2</sub>	NA	TMB	1.83	4.31	NA	Lin et al., 2014b
		H <sub>2</sub> O <sub>2</sub>	0.24	4.52		
MoSe <sub>2</sub>	NA	TMB	0.014	0.56	NA	Wu et al., 2018
		H <sub>2</sub> O <sub>2</sub>	0.155	0.99		
WSe <sub>2</sub>	NA	TMB	0.0433	1.43	NA	Chen T. M. et al., 2017
		H <sub>2</sub> O <sub>2</sub>	19.53	2.22		
VS <sub>2</sub>	NA	TMB	0.28	41.6	NA	Huang et al., 2018
		H <sub>2</sub> O <sub>2</sub>	3.49	55.7		
PtAg/MoS <sub>2</sub>	NA	TMB	25.71	7.29	NA	Cai et al., 2016
		H <sub>2</sub> O <sub>2</sub>	0.386	3.22		
N-doped MoS <sub>2</sub>	NA	TMB	0.7916	1.796	NA	Feng et al., 2020
		H <sub>2</sub> O <sub>2</sub>	0.4459	4.348		
NiFe LDHs	NA	TMB	0.5 ± 0.05	NA	NA	Zhan et al., 2018
		H <sub>2</sub> O <sub>2</sub>	2.4 ± 0.1			
CeO <sub>2</sub> /CoFe LDHs	NA	TMB	0.419	NA	NA	Yang et al., 2020
		H <sub>2</sub> O <sub>2</sub>	10.82			
AuNi/g-C <sub>3</sub> N <sub>4</sub>	NA	TMB	0.16	2.34	NA	Darabdhara et al., 2019
		H <sub>2</sub> O <sub>2</sub>	4.47	6.16		
Au/g-C <sub>3</sub> N <sub>4</sub>	NA	TMB	0.27	1.27	NA	Darabdhara et al., 2019
		H <sub>2</sub> O <sub>2</sub>	11.13	3.44		
Ni/g-C <sub>3</sub> N <sub>4</sub>	NA	TMB	0.49	0.75	NA	Darabdhara et al., 2019
		H <sub>2</sub> O <sub>2</sub>	19.91	1.38		
MOF	NA	TMB	0.365	6.53	NA	Chen J. Y. et al., 2018
		H <sub>2</sub> O <sub>2</sub>	2.49	130		
h-BN	NA	TMB	0.42	NA	NA	Ivanova et al., 2019
		H <sub>2</sub> O <sub>2</sub>	12.2			
Pt/h-BN	NA	TMB	0.21	NA	NA	Ivanova et al., 2019
		H <sub>2</sub> O <sub>2</sub>	9.2			
WO <sub>3</sub>	NA	TMB	10.6	1.53	NA	Li et al., 2019
		H <sub>2</sub> O <sub>2</sub>	1260	3		
Pt/CuO	NA	TMB	0.413	14.6	NA	Wang X. H. et al., 2017
		H <sub>2</sub> O <sub>2</sub>	2.887	8.85		
Pd	NA	TMB	0.21	7.01	NA	Cai et al., 2020
		H <sub>2</sub> O <sub>2</sub>	4.44	4.02		
Pd	5.06	TMB	0.1098	5.82	1.2	Wei et al., 2015
		H <sub>2</sub> O <sub>2</sub>	4.398	6.51	1.3	

(Continued)

TABLE 1 | Continued

Catalyst	[E] (10 <sup>-12</sup> M)	Substrate	K <sub>m</sub> (mM)	V <sub>max</sub> (10 <sup>-8</sup> M S <sup>-1</sup> )	K <sub>cat</sub> (10 <sup>4</sup> s <sup>-1</sup> )	References
Au/Pd	NA	TMB	0.295	19.65	NA	Cai et al., 2020
		H <sub>2</sub> O <sub>2</sub>	5.89	8.19		
Pt/Pd	1.9	TMB	0.0865	6.228	3.1	Wei et al., 2015
		H <sub>2</sub> O <sub>2</sub>	2.231	5	2.5	
Rh	1.53	TMB	0.264	12.56	8.2	Cai et al., 2018b
		H <sub>2</sub> O <sub>2</sub>	4.51	68.09	44.5	

<sup>a</sup>K<sub>cat</sub> = V<sub>max</sub>/E, where E is the concentration of the catalyst.  
Not available, NA.

of H<sub>2</sub>O<sub>2</sub> molecules are broken to generate ·OH radicals, which subsequently oxidize the substrates. In a representative example, Yang's group found that after the coverage of Au NPs onto the g-C<sub>3</sub>N<sub>4</sub> NSs (Wu et al., 2019), the generation of ·OH radicals remarkably increased during catalysis, evidenced by electron spin resonance (ESR). The increase in ·OH radicals could be attributed to the synergistic effect of Au NPs and g-C<sub>3</sub>N<sub>4</sub> NSs, which enhanced the POD-catalysis. By contrast, for the latter, the 2D NMs mediate ET between the substrates and H<sub>2</sub>O<sub>2</sub> molecules, instead of ROS generation. Take the Au NPs coated Pd NSs reported by our group (Cai et al., 2020) for example, with the introduction of Au atoms, the electronic structure of Pd NSs was modified, which subsequently caused a change in the catalytic pathway of Pd NSs (i.e., from ·OH generation to rapid ET process).

Different from PODs, ODs catalyze oxidations with O<sub>2</sub> as the oxygen source (generally in the open air), instead of unstable H<sub>2</sub>O<sub>2</sub>. The potential oxidative damage of biological species by H<sub>2</sub>O<sub>2</sub> could also be avoided by the use of O<sub>2</sub>. The metal oxide NSs like MnO<sub>2</sub> NSs (Liu et al., 2017; Yan et al., 2017; Ge et al., 2019) were found to exhibit OD-like activities, with the merits of operational simplicity and fine compatibility. Besides, good stability of MnO<sub>2</sub> NSs as OD-mimics was also found by several research groups. For example, Dyson's group synthesized the MnO<sub>2</sub> NSs by exfoliation of bulk δ-MnO<sub>2</sub> in BSA aqueous solution (Liu et al., 2017). After storage for 3 months, no significant loss in the activity of NSs was observed. Similar findings were obtained from Rh NSs (Cai et al., 2018b) and PtRh/Rh nanocomposites (Cai et al., 2019). In some studies, the OD-catalysis was believed to go through the generation of ROS such as superoxide ions (O<sub>2</sub><sup>·-</sup>), via cleavage of O-O bonds in O<sub>2</sub> molecules (Cai et al., 2019; Ge et al., 2019).

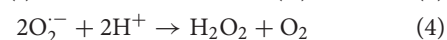
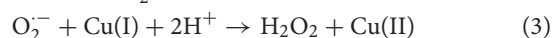
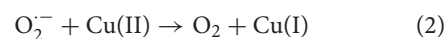
Notably, besides temperature and substrate concentration, the POD/OD-like activities of 2D nanozymes greatly depend on system pH (often around 4 is efficient), which is similar to the 0D examples and enzymes. Thus, to facilitate their application in biosystems, it is highly desirable to develop 2D nanozymes with a wide range of pH, especially at neutral pH. In an early study, Qu's group synthesized the lysozyme-stabilized Au clusters on GO NSs (Au/GO), which exhibited good catalytic activity over a broad pH range, even in physiological pH (Tao et al., 2013). Compared to that at pH 3.0, the POD-like activity of Au/GO remained about 82 % at pH 7.0. In a recent study, Kim's group

reported the rosette-shaped C<sub>3</sub>N<sub>4</sub> by the polymerization reaction between cyanuric acid and melamine, followed by calcination (Heo et al., 2020). Due to larger surface area and higher porosity, the activity of as-prepared materials was appropriately 10-fold higher than that of conventional bulk-C<sub>3</sub>N<sub>4</sub>. Interestingly, the maximal activity was shown at pH 8.0, and over 80% of the activity relative to the maximum activity remained across a pH range of 6.0–9.0.

Although numerous 2D nanozymes exhibited high activity, the catalysis is also lacking selectivity, similar to the 0D ones. To this end, Lee's group synthesized the N- and B-codoped rGO NSs, which showed high efficiency in POD-catalysis, nearly 1000-fold higher than that of undoped rGO (Kim et al., 2019). More importantly, no OD-like activity was observed for the as-prepared materials, suggesting high selectivity. The same group also provided another valuable example, in which the Fe-N<sub>4</sub> single site, resembled the heme cofactor present in HRP, was embedded in graphene to obtain the Fe-N-rGO nanocomposites (Kim et al., 2020). Intriguingly, the nanocomposites not only showed a remarkable enhancement in catalytic efficiency, up to appropriately 700-fold higher than that of undoped rGO but had excellent selectivity toward H<sub>2</sub>O<sub>2</sub>. The single-atom nanozymes (SAzymes), as a very new concept in the nanozyme field (Jiao et al., 2019), could open a window to develop a new type of highly active and selective 2D hybrid nanozymes at the atomic scale.

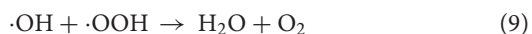
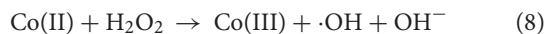
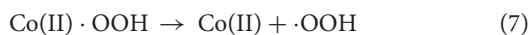
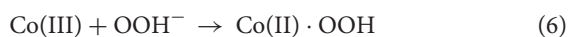
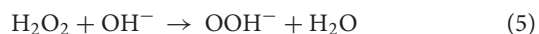
## SOD- and CAT-Like Properties

Contrary to oxidative biocatalysts, SODs and CATs are a type of antioxidant enzyme, which plays an essential part in maintaining redox balance in living organisms by scavenging excess ROS (Liu Y. et al., 2014). There are three forms of human SODs [i.e., cytosolic CuZn SOD, mitochondrial Mn SOD, and extracellular SOD, of which the first is the most studied (Korschelt et al., 2017)]. In a typical cycle of CuZn SOD (Yu et al., 2014; Korschelt et al., 2017), the metal Cu center shuttles between the Cu<sup>2+</sup>/Cu<sup>+</sup> redox states (Equations 2, 3), catalyzing the disproportionation of O<sub>2</sub><sup>·-</sup> into O<sub>2</sub> and H<sub>2</sub>O<sub>2</sub> under neutral conditions (Equation 4).



Following a similar mechanism to that described above, several NMs based on  $V_2O_5$  nanowires (Vernekar et al., 2014) and  $CeO_2$  NPs (Korsvik et al., 2007) have displayed intrinsic SOD-like activities. The polyvinylpyrrolidone (PVP)-modified  $Nb_2C$  NSs obtained by liquid-phase exfoliation (Ren et al., 2019) also provide an interesting example of SOD-mimics. By density functional theory (DFT) calculations together with the characterization of active intermediates via X-ray photoelectron spectroscopy (XPS) and X-ray diffraction (XRD) analysis, the authors discovered the SOD-like activity of  $Nb_2C$  NSs originated from the surface oxidation process, in which  $Nb_2O_5$  formed as catalytically active species.

CATs accelerate the dismutation of  $H_2O_2$  into  $O_2$  and  $H_2O$ , often in the reaction solutions at a high pH (Wei and Wang, 2013; Huang et al., 2019; Jiang D. W. et al., 2019). Previous studies have revealed that the CAT-like activities of 0D metal oxide NPs originated from ion pairs (catalytic sites in two different oxidation states), such as  $Co^{2+}/Co^{3+}$  (Mu et al., 2013),  $Fe^{2+}/Fe^{3+}$  (Lin and Gurol, 1998), and  $Mn^{3+}/Mn^{4+}$  (Hasan et al., 1999). Take  $Co_3O_4$  NPs (Mu et al., 2013) for example, the catalytic mechanism can be described as follows. Under alkaline conditions, it is believed that there is a larger concentration of perhydroxyl anions ( $OOH^-$ ) in the reaction system (Equation 5) (Mu et al., 2013). Since  $OOH^-$  radicals are more nucleophilic than  $H_2O_2$  molecules, they could readily interact with Co(III) centers (Equation 6) to generate Co(II) species and release  $\cdot OOH$  radicals (Equation 7), while  $H_2O_2$  molecules were activated by Co(II) center to produce  $\cdot OH$  radicals (Equation 8). The coupling reaction of the generated  $\cdot OH$  and  $\cdot OOH$  radicals gave water and oxygen as final products (Equation 9).



The above mechanism could also apply to 2D counterparts. For example, Jiang's group prepared MnFe LDHs by simple coprecipitation, which exhibited intrinsic CAT-like activities (Ruan et al., 2018). The authors explained that both the  $Mn^{3+/4+}$  and  $Fe^{3+}$  species exhibited catalytic activity toward  $H_2O_2$ , which could be used for  $H_2O_2$  decomposition to generate oxygen in cancer tissues, to enhance the effect of oxygen-dependent photodynamic therapy (PDT). In another study, besides the metal center shuttling during catalysis, Zheng's group demonstrated the role of ligands in the CAT-like activity of MOF NSs. The Cu MOF NSs were synthesized based on the coordination reaction between the  $Cu^{2+}$  ions and isophthalic acids as ligands, with different substituent groups (e.g.,  $-CH_3$ ,  $-NO_2$ ,  $-OH$ , and  $-NH_2$ ) at 5-position (Wang et al., 2019). The authors found that the CAT-like activity of as-obtained materials was related to the charge density around Cu atoms in the NSs, in which the nitro-functionalized NSs exhibited the highest activity. Since the nitro group is an electron-drawing group while

other groups are electron-donating ones, the positive charge density around Cu atoms for the nitro-modified NSs was the highest, which was favorable for the binding of  $H_2O_2$  as an electron donor.

It is also of note that several 2D NMs were found to have multiple enzymatic activities. For example, Yang's group found that the few-layer  $MoS_2$  NSs prepared by liquid-exfoliation exhibited ternary activities (POD-, OD-, and CAT-like activities) (Chen T. M. et al., 2018). As discussed above, these enzymatic activities could be closely associated with specific reaction conditions especially system pH, in which the acidic conditions are usually favorable for POD/OD-mimic catalysis (Qi et al., 2016; Cai et al., 2017; Darabdharma et al., 2019; Feng et al., 2020), while a high pH is beneficial to CAT-catalysis (Liu Y. et al., 2014; Ruan et al., 2018; Wang et al., 2019). Due to the use of various 2D NMs in biomedical fields, for a meaningful discussion of enzyme-like activity, the reaction parameters, nature of materials (e.g., morphology, structure, composition, and size), capping agents, and surface charge, are believed to be taken into account (Cai and Yang, 2020).

## BIOMEDICAL APPLICATIONS OF 2D NANOZYMES

### Toxicology of 2D NMs

To access the full potential of 2D NMs for practical applications, it is necessary to know their toxicity, including *in vitro* cellular uptake, location, toxicity, *in vivo* biodistribution, degradation, and excretion. However, to date, few studies have highlighted biocompatibility.

The *in vitro* biocompatibility of graphene-based materials, as the oldest and most studied 2D examples, was found to be highly related to their structural/compositional parameters and physicochemical properties, such as morphology, size, layer numbers, hydrophobicity/hydrophilicity, dispersion, and concentration (Ghosal and Sarkar, 2018). For example, hydrophobic and large-size graphene had higher cytotoxicity than hydrophilic and nanosized counterparts (Sukumar et al., 2020). Cui's group found that the cytotoxicity of GO was affected by their concentration, in which the presence of GO with a low concentration ( $<10 \mu g mL^{-1}$ ) slightly decreased the viability of human fibroblast cells ( $<20\%$  when exposed for 4 days), but high concentrations of graphene ( $>50 \mu g mL^{-1}$ ) showed obvious cytotoxicity even after only 1 day of exposure ( $>20\%$ ) (Wang et al., 2011). This was caused by the agglomerates of the physiological medium formed between GO layers *via*  $\pi - \pi$  interactions. Since the aggregated macroparticles could not enter into the cells, they became entrapped on the cell membrane and gave rise to cytoskeleton disruption, membrane deformation, and an increase in intercellular stress, ultimately resulting in cell death. In addition, Koyakutty's group observed that the cytotoxicity of pristine graphene could be improved by carboxyl functionalization (Sasidharan et al., 2011). As the concentration of pristine graphene increased from 0 to  $300 \mu g mL^{-1}$ , the viability of Vero cells decreased remarkably. A lower concentration of pristine graphene ( $100 \mu g mL^{-1}$ ) resulted in

the death of appropriately 50% of cells, which further increased to about 60% at  $300 \mu\text{g mL}^{-1}$ . Contrarily, the functionalized graphene showed negligible effects on the viability, even at the highest concentration studied. In another study by the same group, functionalized hydrophilic graphene was found to be favorable for macrophage cell (RAW 264.7) uptake (Sasidharan et al., 2012), distinct from the hydrophobic pristine graphene. The pristine graphene was primarily accommodated at the cell surface and induced ROS-mediated apoptosis when the concentration was above  $50 \mu\text{g mL}^{-1}$ , which has not been found for functionalized graphene at a higher concentration of  $75 \mu\text{g mL}^{-1}$ . Despite enhanced cytocompatibility by surface functionalization, all forms of graphene-based materials could lead to ROS generation in mammalian cells, which should be carefully taken into account for biomedical applications (Liao et al., 2011; Gollavelli and Ling, 2012).

In an earlier study on the *in vivo* biodegradability of graphene, Koyakutty's group revealed that time-bound spectral alternations using confocal Raman imaging, such as the formation of the defective  $D'$  band, widening of D and G bands, and increase in  $I_D/I_G$  ratio of pristine graphene, embedded in different organs (e.g., lung, liver, kidney, and spleen of mice) over a time of 8–90 days (Girish et al., 2013). These observations arose from the increase in structural disorders in graphene phagocytosed by macrophages. The most enhanced amount of disorder, which was observed for the spleen bound samples, caused complete amorphization after 90 days of intravenous injection. In another study, after intravenous GO administration, the accumulation of GO was increased largely in the lung and liver for a longer time (Liu et al., 2012). GO NSs accumulated because of the possible instability and nonspecific binding of GO with different proteins. Since the blood initially flowed to the lung, more GO NSs were accumulated in the lung than other organs. Dash's group investigated the effect of GO and rGO on blood platelet functions (Singh et al., 2011). In this study, the GO sheets were found to cause strong aggregatory responses in platelets by activating a family of Src kinases, which further led to the release of calcium from intercellular compartments. Moreover, this study revealed that, due to charge distribution on the surface of GO NSs, the intravenous administration of GO in mice could trigger pulmonary thromboembolism. By contrast, rGO was unable to effectively activate platelets because of reduced charge density on the graphene surface.

The exploration of TMDs in biomedical areas began in 2013–2014. Similar to graphene-based materials, after surface modification, several members of TMDs also showed good *in vitro* biocompatibility. A relevant example is the  $\text{WS}_2$  NSs prepared by Liu's group using the Li ions insertion method (Cheng et al., 2014). Without surface modification, the authors found that the  $\text{WS}_2$  NSs exhibited obvious toxicity toward 4T1 (murine breast cancer cells), HeLa (human epithelial carcinoma cells), and 293T (human embryo kidney cells) after incubation for 24 h. At a high concentration of  $0.1 \text{ mg mL}^{-1}$  of  $\text{WS}_2$  NSs, only about 50% of cells were alive; however, after modification with PEG, the as-obtained NSs demonstrated no significant cytotoxicity under the same conditions. Contrarily, without

surface functionalization, Zhao's group prepared the  $\text{WS}_2$  NSs by  $\text{H}_2\text{SO}_4$  intercalation and exfoliation in an aqueous solution, which showed low toxicity toward HeLa cells (Yong et al., 2014). The cell viability remained high (above 85%) even at a high concentration ( $0.2 \text{ mg mL}^{-1}$ ). The authors outlined that the biocompatibility of unmodified  $\text{WS}_2$  NSs could be attributed to a mild aqueous phase in synthesis, in which the toxic organic solvents/chemicals were unnecessary. Using a similar method, Zhao's group prepared  $\text{MoS}_2$  NSs, followed by coating with chitosan (Yin et al., 2014). Even at a high concentration up to  $0.4 \text{ mg mL}^{-1}$ , the as-obtained NSs demonstrated low cytotoxicity against KB (human epithelial carcinoma cell line) and Panc-1 (pancreatic carcinoma, epithelial-like cell line). The functionalized NSs also showed negligible hemolysis of red blood cells (RBCs), suggesting good blood compatibility. The above studies revealed that the *in vitro* toxicity of TMDs could be affected by synthetic methodology, surface chemistry, and specific cells. For the investigations on *in vivo* biocompatibility, Liu's group evaluated the toxicity of PEGylated  $\text{WS}_2$  NSs (Cheng et al., 2014) toward Balb/c mice, by hematoxylin and eosin (H&E) assay, serum biochemistry assay, and complete blood panel test. In their study, no obvious abnormal behavior of mice at the dose of  $20 \text{ mg kg}^{-1}$  was observed during the assay (45 days after photothermal therapy). In a similar study by the same group, the PEGylated  $\text{MoS}_2$  NSs also demonstrated no obvious toxicity against Balb/c mice, at a relatively lower dose of  $3.4 \text{ mg kg}^{-1}$  (Liu T. et al., 2014). However, to fully understand their potential toxicity/metabolism in longer terms, more studies are needed.

Compared to graphene-based materials and TMDs, the biocompatibility/biosafety of other 2D NMs especially Xenes, MXenes, and ultrathin metallic NSs, is less explored. Considering these structural and compositional differences, their solubility, biodegradation, and biocompatibility could be different from each other. Presently, the evaluations of *in vitro/vivo* biocompatibility of these materials are in progress (Wang S. G. et al., 2020). Despite the low toxicities of several types of 2D NMs [e.g.,  $\text{MnO}_2$  (Gao et al., 2020),  $g\text{-C}_3\text{N}_4$  (Liang et al., 2017), and  $h\text{-BN}$  (Mateti et al., 2018)] exhibited in preliminary investigations, it is too soon to confirm the biosafety of 2D NMs at this stage. Thus, careful systematic tests on their toxicity are required before practical applications can be developed.

## Biomedical Applications of 2D Nanozymes Biosensors

The accurate determination of biologically important analytes is of significance for clinical diagnosis. The colorimetric method, as an appealing one for point-of-care (POC) applications with many merits (e.g., low cost, simplicity, and practicality), has attracted considerable interest in biosensing (Song et al., 2011).

With good stability and adjustable catalytic activities, 2D NMs provide useful platforms for *in vitro* colorimetric detection. Recently, the assays for various bioanalytes like small molecules, cancer cells, and ions, have been proposed based on POD-like activities of 2D NMs (Table 2). As a typical example, the colorimetric assays for glucose have been largely developed based



**TABLE 2** | Summary of several typical 2D nanozymes for colorimetric detection of various target analytes.

Analyte	Materials	Activity	LDR	LOD	References
Glucose	GO	POD	1–20 $\mu\text{M}$	1 $\mu\text{M}$	Song et al., 2010
Glucose	FePd/rGO	POD	1–200 $\mu\text{M}$	1.76 $\mu\text{M}$	Yang et al., 2019
Glucose	MoS <sub>2</sub>	POD	5–150 $\mu\text{M}$	1.2 $\mu\text{M}$	Lin et al., 2014a
Glucose	WS <sub>2</sub>	POD	5–300 $\mu\text{M}$	2.9 $\mu\text{M}$	Lin et al., 2014b
Glucose	WSe <sub>2</sub>	POD	10–60 $\mu\text{M}$	10 $\mu\text{M}$	Chen T. M. et al., 2017
Glucose	VS <sub>2</sub>	POD	5–250 $\mu\text{M}$	1.5 $\mu\text{M}$	Huang et al., 2018
Glucose	PtAg/MoS <sub>2</sub>	POD	1–10 $\mu\text{M}$	0.8 $\mu\text{M}$	Cai et al., 2016
Glucose	NiFe LDHs	POD	0.05–2.0 mM	23 $\pm$ 2 $\mu\text{M}$	Zhan et al., 2018
Glucose	CeO <sub>2</sub> /CoFe	POD	0.05–2.0 mM	15 $\mu\text{M}$	Yang et al., 2020
Glucose	<i>g</i> -C <sub>3</sub> N <sub>4</sub>	POD	5–100 $\mu\text{M}$	1.0 $\mu\text{M}$	Lin et al., 2014c
Glucose	Au/ <i>g</i> -C <sub>3</sub> N <sub>4</sub>	POD	5–100 $\mu\text{M}$	1.2 $\mu\text{M}$	Wu et al., 2019
Glucose	Pd/ <i>g</i> -C <sub>3</sub> N <sub>4</sub>	POD	50–2,000 $\mu\text{M}$	50 $\mu\text{M}$	Zhang W. C. et al., 2019
Glucose	Fe/ <i>g</i> -C <sub>3</sub> N <sub>4</sub>	POD	0.5–10 $\mu\text{M}$	0.5 $\mu\text{M}$	Tian et al., 2013
Glucose	AuNi/ <i>g</i> -C <sub>3</sub> N <sub>4</sub>	POD	0.5–30 $\mu\text{M}$	1.7 $\mu\text{M}$	Darabdhara et al., 2019
Glucose	Au/Pd	POD	5–400 $\mu\text{M}$	0.85 $\mu\text{M}$	Cai et al., 2020
Glucose	Pt/Pd	POD	0.1–0.5 mM	NA	Wei et al., 2015
Glucose	Au/MOF	GOx, POD	10–300 $\mu\text{M}$	8.5 $\mu\text{M}$	Huang et al., 2017a
AA	Pt/CuO	POD	1 $\mu\text{M}$ –0.6 mM	0.796 $\mu\text{M}$	Wang X. H. et al., 2017
AA	IrO <sub>2</sub> /GO	POD	5–70 $\mu\text{M}$	324 nM	Sun et al., 2020
GSH	MnO <sub>2</sub>	OD	NA	300 nM	Liu et al., 2017
GSH	MnO <sub>2</sub>	OD	10 nM–5 $\mu\text{M}$	5.6 nM	Ge et al., 2019
GSH	IrO <sub>2</sub> /rGO	POD	0.1–50 $\mu\text{M}$	83 nM	Liu X. L. et al., 2019
Cysteine	IrO <sub>2</sub> /rGO	POD	0.1–50 $\mu\text{M}$	40 nM	Liu X. L. et al., 2019
Homocysteine	IrO <sub>2</sub> /rGO	POD	0.1–50 $\mu\text{M}$	57 nM	Liu X. L. et al., 2019
Xanthine	Rh	POD	2–80 $\mu\text{M}$	0.73 $\mu\text{M}$	Cai et al., 2018b
Xanthine	WO <sub>3</sub>	POD	25–200 $\mu\text{M}$	1.24 $\mu\text{M}$	Li et al., 2019
Xanthine	MoSe <sub>2</sub>	POD	0.01–0.32 mM	1.964 $\mu\text{M}$	Wu et al., 2018
Dopamine	Pt/BN	POD	2–55 $\mu\text{M}$	0.76 $\mu\text{M}$	Ivanova et al., 2019
Dopamine	CuS/rGO	POD	2–100 $\mu\text{M}$	0.48 $\mu\text{M}$	Dutta et al., 2015
Cholesterol	CuS/BN	POD	10–100 $\mu\text{M}$	2.9 $\mu\text{M}$	Zhang et al., 2017
AChE	MnO <sub>2</sub>	OD	0.1–15 mU mL <sup>-1</sup>	35 $\mu\text{U mL}^{-1}$	Yan et al., 2017
MCF-7 cells	Au/GO	POD	NA	1,000	Tao et al., 2013
MCF-7 cells	PtCu/MoS <sub>2</sub>	OD	NA	300	Qi et al., 2016
MCF-7 cells	Pt/GO	POD	NA	125	Zhang L. N. et al., 2014
S <sup>2-</sup> ions	MoS <sub>2</sub> / <i>g</i> -C <sub>3</sub> N <sub>4</sub>	POD	0.1–10 $\mu\text{M}$	37 nM	Liu et al., 2020
Fe <sup>2+</sup> ions	MoS <sub>2</sub>	POD	0.01–0.8 $\mu\text{M}$	7 nM	Wang et al., 2016
Pb <sup>2+</sup> ions	WS <sub>2</sub>	POD	5–80 $\mu\text{g L}^{-1}$	4 $\mu\text{g L}^{-1}$	Tang et al., 2020

<sup>a</sup>Acetylcholinesterase.

AChE, Linear detection range; LDR, Limit of detection, LOD.

on a host of 2D NMs and their hybrids, including graphene derivatives [e.g., GO (Song et al., 2010), FePd/rGO (Yang et al., 2019)], TMDs [e.g., MoS<sub>2</sub> (Lin et al., 2014a), WS<sub>2</sub> (Lin et al., 2014b), WSe<sub>2</sub> (Chen T. M. et al., 2017), VS<sub>2</sub> (Huang et al., 2018)] and their hybrids [e.g., PtAg/MoS<sub>2</sub> (Cai et al., 2016)], LDHs [e.g., NiFe (Zhan et al., 2018)], and their hybrids [e.g., CeO<sub>2</sub>/CoFe (Yang et al., 2020)], *g*-C<sub>3</sub>N<sub>4</sub> (Lin et al., 2014c) and its hybrids [e.g., Au/*g*-C<sub>3</sub>N<sub>4</sub> (Wu et al., 2019), Pd/*g*-C<sub>3</sub>N<sub>4</sub> (Zhang W. C. et al., 2019), Fe/*g*-C<sub>3</sub>N<sub>4</sub> (Tian et al., 2013), and AuNi/*g*-C<sub>3</sub>N<sub>4</sub> (Darabdhara et al., 2019)], and metallic NSs-based hybrids [e.g., Au/Pd (Cai et al., 2020) and Pt/Pd (Wei et al., 2015)].

Some of them showed excellent analytic performance (e.g., wide linear detection range, high sensitivity, and selectivity) for glucose detection and demonstrated practicality and superiority for real samples. However, it is noteworthy that these materials could only be employed to mimic PODs and that glucose oxidase (GOx) was required for detection, since it catalyzed the aerobic oxidation of glucose to generate H<sub>2</sub>O<sub>2</sub>. Intriguingly, Zhang's group proposed a non-enzyme colorimetric assay for glucose based on GOx- and the POD-like activities of Au/MOF, which catalyzed cascade reactions for detection (Huang et al., 2017a). The multifunctional enzymatic properties of

hybridized 2D NMs provide valuable opportunities to develop advanced biosensors.

By taking advantage of POD-/OD-like activity of 2D NMs, the colorimetric assays for other analytes like AA (Wang X. H. et al., 2017; Sun et al., 2020), biothiols [e.g., GSH (Liu et al., 2017; Ge et al., 2019; Liu X. L. et al., 2019), cysteine (Liu X. L. et al., 2019), and homocysteine (Liu X. L. et al., 2019)], xanthine (Cai et al., 2018b; Wu et al., 2018; Li et al., 2019), dopamine (Dutta et al., 2015; Ivanova et al., 2019), cholesterol (Zhang et al., 2017), acetylcholinesterase (Yan et al., 2017), cancer cells (Tao et al., 2013; Zhang L. N. et al., 2014; Qi et al., 2016), ions [e.g.,  $S^{2-}$  (Liu et al., 2020),  $Fe^{2+}$  (Wang et al., 2016), and  $Pb^{2+}$  (Tang et al., 2020)], have also been established by different groups. The colorimetric biosensing based on 2D nanozymes continues to be a rapidly growing field.

### Antibacterial Agents

The POD-like activities of 2D NMs have gained ever-increasing interest in antibacterial applications. For example, Yang's group prepared MoSe<sub>2</sub> NSs by exfoliation of bulk MoSe<sub>2</sub> powder in the aqueous solution of carboxyl-modified silk fibroin under sonication conditions (Huang X.-W. et al., 2017). In their study, a high concentration of H<sub>2</sub>O<sub>2</sub> (100 mM) alone was required to eliminate most Gram-negative bacteria *E. Coli*, while only 100 μM H<sub>2</sub>O<sub>2</sub> could display excellent antibacterial activity in the presence of MoSe<sub>2</sub> NSs (50 μg mL<sup>-1</sup>). The effectiveness of a combination of MoSe<sub>2</sub> NSs and H<sub>2</sub>O<sub>2</sub> was further verified for disinfection and healing of Kunming mice with infected skin wounds. The study provided a type of TMD-based antibacterial agents with the usage of low-dose H<sub>2</sub>O<sub>2</sub>, which potentially avoid the harmful side effects of high-dose H<sub>2</sub>O<sub>2</sub> in traditional medical therapy. Similarly, Yin's group (Ma D. Q. et al., 2020) and Gu's group (Wang T. et al., 2020) respectively reported good antibacterial efficacy of lysozyme-modified MoS<sub>2</sub> NSs and N-doped MoS<sub>2</sub> or WS<sub>2</sub> NSs, against *E. Coli* and Gram-positive *Bacillus subtilis*. The POD-mimics catalyzed H<sub>2</sub>O<sub>2</sub> decomposition to generate ·OH radicals, which promoted bacteria-infected wound healing. Several 2D hybrid NMs like Au/g-C<sub>3</sub>N<sub>4</sub> (Wang Z. Z. et al., 2017) also showed potential in antibacterial agents.

Recently, Qu's group constructed a self-activated cascade reagent based on GOx-adsorbed 2D Cu-TCPP(Fe) MOF NSs (Figure 2A), which was used together with glucose in the antibacterial system (Liu X. P. et al., 2019). The authors also created the wound model on the back of Kunming mice and prepared a MOF/GOx-band-aid for the *in vivo* bacterial study (Figure 2B). The principle was based on the consecutive reactions, in which GOx firstly catalyzed the oxidation of glucose to gluconic acid and H<sub>2</sub>O<sub>2</sub>, which was further catalytically decomposed into ·OH radicals by MOF NSs as a POD-mimic, thus leading to an antibacterial effect and ultimately, wound healing (Figure 2C). In the *in vitro* antibacterial investigation, the group (glucose + MOF/GOx) led to high bacteria inactivation rates, up to 88% and 90 % for *E. Coli* and *S. aureus*, respectively. By contrast, for the control groups including (1) PBS, (2) glucose, (3) glucose + MOF, and (4) MOF/GOx, the viabilities remained above 50% for the two bacteria. In the *in vivo* antibacterial study, the bacteria for the group (glucose + MOF/GOx-band-aid) were

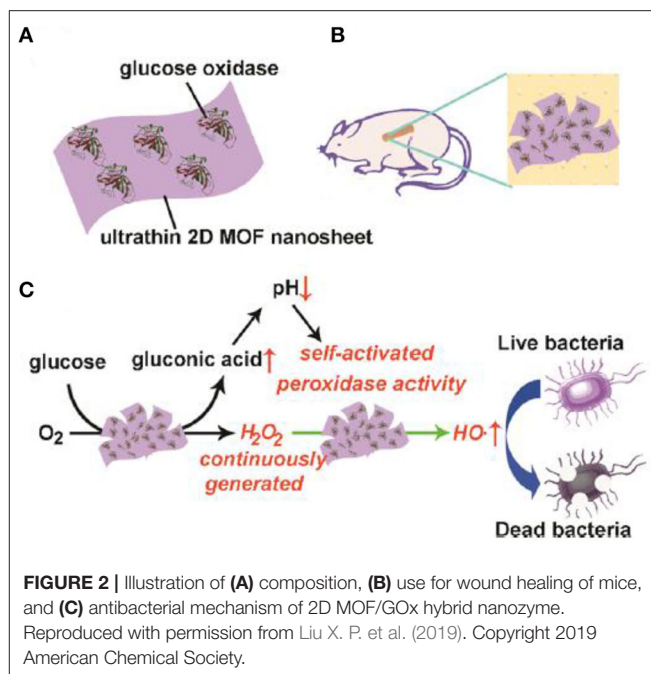


**FIGURE 2** | Illustration of (A) composition, (B) use for wound healing of mice, and (C) antibacterial mechanism of 2D MOF/GOx hybrid nanozyme. Reproduced with permission from Liu X. P. et al. (2019). Copyright 2019 American Chemical Society.

decreased to 9.1%; however, the bacteria for the control group (glucose + GOx-band-aid) were only decreased to 56.5%. These results showed high antibacterial activity of MOF/GOx. More interestingly, since H<sub>2</sub>O<sub>2</sub> is an oxidant that was continuously produced by oxidation of glucose in the cascade catalysis, the study provided a benign antibacterial system to avoid the direct introduction of highly concentrated H<sub>2</sub>O<sub>2</sub>.

### Antioxidants

2D NMs had important applications in antioxidants. Table 3 shows a summary of 2D nanozymes as antioxidants. Typical examples include GO NSs (Halim et al., 2019), Se NPs *in situ* grown on GO NSs (Huang et al., 2017b), and MoS<sub>2</sub> NSs prepared by sonication-assisted exfoliation (Chen T. M. et al., 2018). In another example, the different TMDs (WS<sub>2</sub>, MoSe<sub>2</sub>, and WSe<sub>2</sub>) were functionalized with an amphiphilic poly( $\epsilon$ -caprolactone)-*b*-PEG (PCL-*b*-PEG) diblock copolymer, which efficiently captured mitochondrial and intracellular ROS and reaction nitrogen species (RNS) like ·NO radicals, of which the WS<sub>2</sub> NSs displayed the best performance (Yim et al., 2020). With effective scavenging of ROS and RNS as well as suppression of inflammatory cytokines of WS<sub>2</sub> NSs, the survival rate of the septic mice remarkably increased to 90%.

Chen's group found that the PVP-functionalized Nb<sub>2</sub>C NSs could greatly reduce ROS generation caused by ionizing radiation, thereby providing a kind of antioxidant based on 2D nanozymes for radioprotective applications (Ren et al., 2019). Wang's group also demonstrated the potential of Se-modified g-C<sub>3</sub>N<sub>4</sub> NSs against oxidative stress (Cao X. N. et al., 2020).

### Therapeutics

A new hotspot in nanozyme research is the integration of enzymatic properties for therapy. Using an *in situ* growth strategy, Liu's group fabricated Pt NPs decorated on the surface

**TABLE 3** | Summary of representative 2D nanozymes as antioxidants.

2D NMs	Enzymatic activity	Applications	References
GO NSs	SOD, CAT	Protecting mesenchymal stem cells from ROS accumulation	Halim et al., 2019
Se/GO	Glutathione Peroxidase	protecting RAW264.7 cells from oxidative stress by catalyzing H <sub>2</sub> O <sub>2</sub> decomposition to H <sub>2</sub> O	Huang et al., 2017
MoS <sub>2</sub> NSs	SOD, CAT	Protecting <i>Escherichia coli</i> ( <i>E. coli</i> ), <i>Staphylococcus aureus</i> ( <i>S. aureus</i> ) and A549 cells from H <sub>2</sub> O <sub>2</sub> -induced oxidative stress	Chen T. M. et al., 2018
WS <sub>2</sub> , MoSe <sub>2</sub> and WSe <sub>2</sub> NSs coated with PCL-b-PEG	SOD, CAT	Scavenging mitochondrial and intracellular ROS and RNS in lipopolysaccharide (LPS)- or bacteria-induced inflammatory cells	Yim et al., 2020
PVP-modified Nb <sub>2</sub> C NSs	SOD	Scavenging ROS against ionizing radiation	Ren et al., 2019
Se-modified g-C <sub>3</sub> N <sub>4</sub> NSs	CAT	Protecting A549 cells from ROS-induced damage	Cao X. N. et al., 2020

of black phosphorus (BP) NSs, obtained by the liquid exfoliation method (**Figure 3A**) (Ouyang et al., 2018). The as-obtained BP NSs were freestanding with several hundred nanometers (**Figure 3B**), while the Pt NPs had an average size of appropriately 4.2 nm (**Figure 3C**), with the crystal lattice fringe of 0.223 nm of (111) plane. The element distribution was further obtained from high-angle annular dark-field scanning TEM (HAADF-STEM) image (**Figure 3D**) and element maps (**Figures 3E,F**). The as-obtained Pt/BP nanocomposites integrated CAT-like activity of Pt NPs and photodynamic therapy (PDT) activity of BP NSs, in which the Pt NPs catalytically decomposed the accumulated H<sub>2</sub>O<sub>2</sub> in tumors to relieve tumor hypoxia (**Figure 3A**). In the *in vitro* antitumor experiment, the BP NSs alone only reduced 26% of cell viability under near infrared (NIR) light irradiation, while about 65% of tumor cells were dead after the treatment of the Pt/BP. The result showed that the elevated O<sub>2</sub> level caused by CAT-catalysis of Pt NPs remarkably improved the PDT efficiency of BP NSs. Moreover, as a result of the Pt/BP treatment, the overexpression of hypoxia-inducible factor-1 $\alpha$  (HIF-1 $\alpha$ ), which is associated with therapy resistance in tumor cells, was significantly down-regulated, since the intensity of fluorescence appeared on the tumor slices of mice was decreased by 64% in the immunohistochemical staining experiment. The down-regulation of HIF-1 $\alpha$  by the Pt/BP decreased the tumor apoptotic resistance, which ultimately enhanced the therapeutic effect in the *in vivo* antitumor experiment, in which the growth of the tumor was completely regressed by the treatment of Pt/BP, while the treatment of BP NSs alone only led to a decline in about 47% of average tumor size.

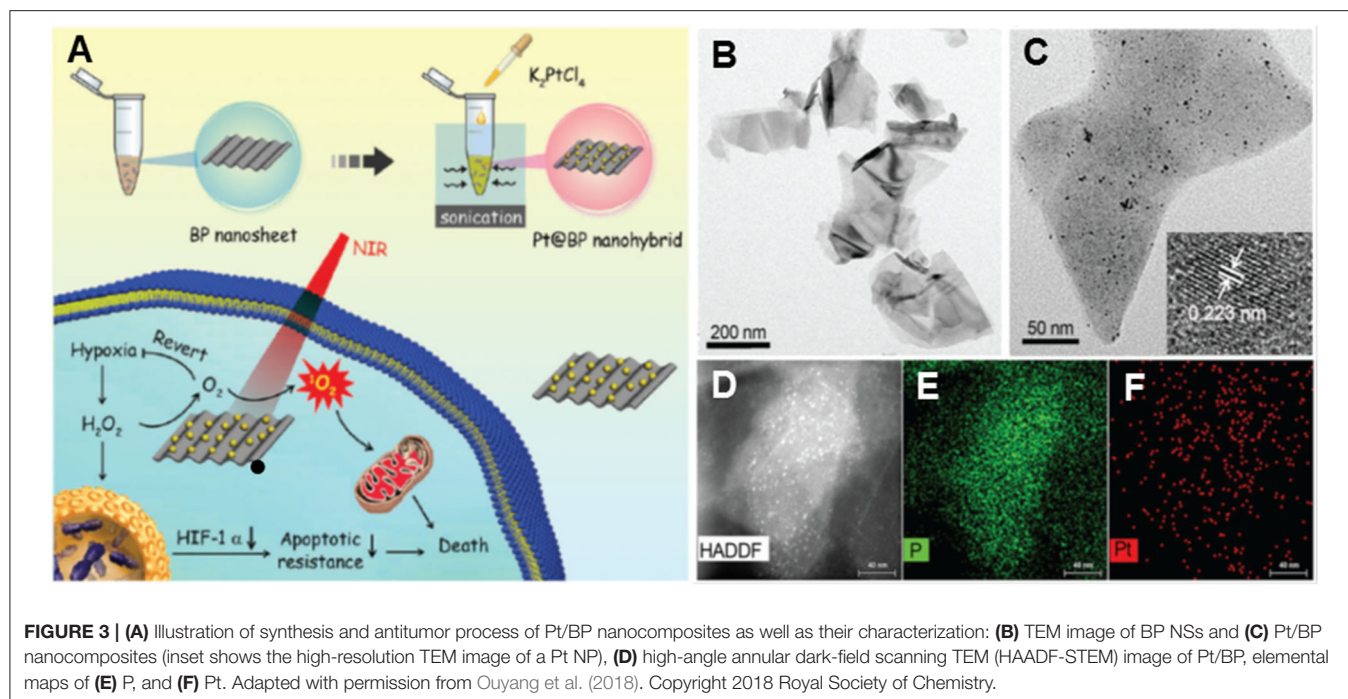
By using a similar *in situ* growth method, Sun's group synthesized Pt NPs coated 2D MOF, that is, Sm-modified tetrakis(4-carboxyphenyl)porphyrin (Sm-TCPP), which afforded

a multifunctional nanozyme with excellent tumor specificity for enhanced PDT efficiency (Cao Z. G. et al., 2020). In their study, the Pt NPs acted as a CAT-mimic, catalyzing over-expressed H<sub>2</sub>O<sub>2</sub> in a tumor microenvironment (TME) into O<sub>2</sub>. The generated O<sub>2</sub> was further catalytically transformed to <sup>1</sup>O<sub>2</sub> by Sm-TCPP, owing to its high ROS generation capacity under light irradiation.

## PROSPECT AND CHALLENGES

This review has undertaken a summary of recent progress in developing 2D NMs with enzyme-like activities for diversified biomedical applications. The continuous advancement of nanoscience and nanotechnology in relation to 2D NMs will offer great opportunities to develop new types of nanozymes with varied functionalities in the future. Meanwhile, the exploration of new biocatalytic properties and integration of enzymatic activities of 2D NMs with other nanostructures like 0D NPs have potentially limitless applications in biomedical areas, and more fundamental technological breakthroughs in 2D nanozymes are expected in the near future.

Despite the many achievements that have been made in research on 2D nanozymes, studies on this field are still in the initial stages and future studies must address some challenges. Firstly, compared to 0D NPs with easy preparation, it is challenging to achieve the controlled synthesis of 2D NMs with uniform thickness, desirable size, and colloidal stability. Despite great success in creating layered materials by the top-down methods, there are still some obvious shortcomings. A typical example is the synthesis of TMDs for biomedical applications, in which the liquid exfoliation and chemical intercalation methods were adopted in most studies. Although the former had a high yield with simple operations, the morphologies of the obtained products had a lack of uniformity, often involving a mixture of single and few-layer sheets with different lateral dimensions (Agarwal and Chatterjee, 2018). Despite the more uniform single-layer NSs created by the latter, it both brought structural and electronic deformations and involved toxic reagents. The chemical intercalation process was highly sensitive to the environment and time-consuming. Therefore, it is still desirable to develop an efficient method to prepare TMDs. Another example is the metallic NSs. Bearing lots of unsaturated atoms, the ultrathin metallic nanostructures are difficult to stabilize, because metal atoms readily form 3D close-packed crystals. Despite tremendous efforts in the synthesis of metallic NSs by bottom-up protocols, the formation mechanism in most reports was proposed based on a simple correlation between a few synthetic parameters and the final shape, in which several characterization techniques (e.g., TEM, XRD, etc.) were employed to identify reaction intermediates, were formed either at certain time intervals or in the control experiments (Chen Y. et al., 2018). However, there is not enough evidence relating to authentic reactive species during synthesis. Therefore, to better understand the formation process (e.g., nucleation, growth, and assembly) of metallic NSs for synthesis, it is essential to carry out



more *in situ* studies on the morphological evolution toward the 2D structure.

Secondly, despite the fascinating enzymatic properties of numerous 2D NMs, few studies on the in-depth catalytic mechanism are available. At present, it is still difficult to predict the nanozyme activity of 2D NMs for a specific structure. It is also difficult to achieve the best performance (e.g., activity and selectivity) for a specific application in biomedical areas, and hard to design the desired 2D nanozymes with optimal structures. Fundamentally, the missing link of structure-property relationship is largely because the enzyme-catalysis mechanism of 2D NMs remains unclear. For example, we must ask what the true active sites of 2D NMs and catalytically active intermediates during enzyme-catalysis are. In this regard, a deeper understanding of the catalytic mechanism of 2D nanozymes could benefit from *in situ* experimental studies and theoretical calculation by establishing appropriate models for catalysis, which are beneficial to the structural design of 2D nanozymes.

Thirdly, unlike 0D nanosystems, the biocompatibility and environmental stability of 2D NMs remains largely unknown, to date. Despite numerous studies on the biocompatibility of graphene-based NMs and TMDSSs, evaluations of the toxicity of other types of 2D NMs are urgently required. The solubility, biodegradation, and biocompatibility of 2D NMs could be different from each other due to differences in their structure, composition, the methodology of synthesis and functionalization, and the cells studied. Therefore, it is hard to speculate whether a specific 2D NM is toxic or not. Their toxicity

(both short-term and long-term), cellular-uptake mechanism, and the metabolic pathways of 2D NMs should be systematically tested for clinical trials.

Finally, it is acknowledged that many of the current applications of 2D nanozymes that display an outstanding performance are just proof-of-concept and have only been performed in laboratories. A number of reports fail to examine processability, scale-up possibility, and cost. The long-term stability and durability of 2D nanozymes are also less explored by researchers. Accordingly, there is still a long way to go before 2D nanozymes can be implemented in practical applications, which ultimately require interdisciplinary collaboration from chemistry, materials science, and biology.

## AUTHOR CONTRIBUTIONS

RY: design the work. SC: drafting the manuscript. All authors contributed to the article and approved the submitted version.

## FUNDING

This work was supported by the Strategic Priority Research Program of the Chinese Academy of Sciences (XDB36000000), the National key research and development program from the Ministry of Science and Technology of China (2016YFC0207102), and the National Natural Science Foundation of China (21503053).

## REFERENCES

- Agarwal, V., and Chatterjee, K. (2018). Recent advances in the field of transition metal dichalcogenides for biomedical applications. *Nanoscale* 10, 16365–16397. doi: 10.1039/C8NR04284E
- Allen, M. J., Tung, V. C., and Kaner, R. B. (2010). Honeycomb carbon: a review of graphene. *Chem. Rev.* 110, 132–145. doi: 10.1021/cr900070d
- Bhimanapati, G. R., Lin, Z., Meunier, V., Jung, Y., Cha, J., Das, S., et al. (2015). Recent advances in two-dimensional materials beyond graphene. *ACS Nano* 9, 11509–11539. doi: 10.1021/acsnano.5b05556
- Butler, S. Z., Hollen, S. M., Cao, L. Y., Cui, Y., Gupta, J. A., Gutiérrez, H. R., et al. (2013). Progress, challenges, and opportunities in two-dimensional materials beyond graphene. *ACS Nano* 7, 2898–2926. doi: 10.1021/nn400280c
- Cai, S. F., Fu, Z., Xiao, W., Xiong, Y. L., Wang, C., and Yang, R. (2020). Zero-dimensional/two-dimensional Au<sub>x</sub>Pd<sub>100-x</sub> nanocomposites with enhanced nanozyme catalysis for sensitive glucose detection. *ACS Appl. Mater. Interfaces* 12, 11616–11624. doi: 10.1021/acsmi.9b21621
- Cai, S. F., Han, Q. S., Qi, C., Lian, Z., Jia, X. H., Yang, R., et al. (2016). Pt<sub>74</sub>Ag<sub>26</sub> nanoparticle-decorated ultrathin MoS<sub>2</sub> nanosheets as novel peroxidase mimics for highly selective colorimetric detection of H<sub>2</sub>O<sub>2</sub> and glucose. *Nanoscale* 8, 3685–3693. doi: 10.1039/C5NR08038J
- Cai, S. F., Han, Q. S., Qi, C., Wang, X. H., Wang, T., Jia, X. H., et al. (2017). MoS<sub>2</sub>-Pt<sub>3</sub>Au<sub>1</sub> nanocomposites with enhanced peroxidase-like activities for selective colorimetric detection of phenol. *Chin. J. Chem.* 35, 605–612. doi: 10.1002/cjoc.201600694
- Cai, S. F., Lian, C., Duan, H. H., Xiao, W., Han, Q. S., Qi, C., et al. (2019). Facile strategy to prepare Rh nanosheet-supported PtRh nanoparticles with synergistically enhanced catalysis in oxidation. *Chem. Mater.* 31, 808–818. doi: 10.1021/acs.chemmater.8b03889
- Cai, S. F., Liu, X. L., Han, Q. S., Qi, C., Yang, R., and Wang, C. (2018a). A novel strategy to construct supported Pd nanocomposites with synergistically enhanced catalytic performances. *Nano Res.* 11, 3272–3281. doi: 10.1007/s12274-017-1868-9
- Cai, S. F., Xiao, W., Duan, H. H., Liang, X. X., Wang, C., Yang, R., et al. (2018b). Single-layer Rh nanosheets with ultrahigh peroxidase-like activity for colorimetric biosensing. *Nano Res.* 11, 6304–6315. doi: 10.1007/s12274-018-2154-1
- Cai, S. F., and Yang, R. (2020). Noble Metal-Based Nanozymes. in: *Nanozymology. Nanostructure Science and Technology*, eds X. Y. Yan (Singapore: Springer), 331–365. doi: 10.1007/978-981-15-1490-6\_10
- Cao, X. N., Lian, S., Tong, Y. W., Lin, W., Jia, L., Fang, Y. X., et al. (2020). Fluorescent Se-modified carbon nitride nanosheets as biomimetic catalases for free-radical scavenging. *Chem. Commun.* 56, 916–919. doi: 10.1039/C9CC08665J
- Cao, Z. G., Li, Y. J., Zhang, Y., Cheng, K. W., An, P. J., Chen, F. H., et al. (2020). Biomimetic platinum nanozyme immobilized on 2D metal-organic frameworks for mitochondrion-targeting and oxygen self-supply photodynamic therapy. *ACS Appl. Mater. Interfaces* 12, 1963–1972. doi: 10.1021/acsmi.9b14958
- Chen, J. Y., Shu, Y., Li, H. L., Xu, Q., and Hu, X. Y. (2018). Nickel metal-organic framework 2D nanosheets with enhanced peroxidase nanozyme activity for colorimetric detection of H<sub>2</sub>O<sub>2</sub>. *Talanta* 189, 254–261. doi: 10.1016/j.talanta.2018.06.075
- Chen, M. M., Wei, D., Chu, W., Wang, T., and Tong, D. G. (2017). One-pot synthesis of O-doped BN nanosheets as a capacitive deionization electrode for efficient removal of heavy metal ions from water. *J. Mater. Chem. A* 5, 17029–17039. doi: 10.1039/C7TA05459A
- Chen, T. M., Wu, X. J., Wang, J. X., and Yang, G. W. (2017). WSe<sub>2</sub> few layers with enzyme mimic activity of high-sensitive and high-selective visual detection of glucose. *Nanoscale* 9, 11806–11813. doi: 10.1039/C7NR03179C
- Chen, T. M., Zou, H., Wu, X. J., Liu, C. C., Situ, B., Zheng, L., et al. (2018). Nanozymatic antioxidant system based on MoS<sub>2</sub> nanosheets. *ACS Appl. Mater. Interfaces* 10, 12453–12462. doi: 10.1021/acsmi.8b01245
- Chen, Y., Fan, Z. X., Zhang, Z. C., Niu, W. X., Li, C. L., Yang, N. L., et al. (2018). Two-dimensional metal nanomaterials: synthesis, properties, and applications. *Chem. Rev.* 118, 6409–6455. doi: 10.1021/acs.chemrev.7b00727
- Chen, Y., Tan, C. L., Zhang, H., and Wang, L. Z. (2015). Two-dimensional graphene analogues for biomedical applications. *Chem. Soc. Rev.* 44, 2681–2701. doi: 10.1039/C4CS00300D
- Cheng, L., Liu, J. J., Gu, X., Gong, H., Shi, X. Z., Liu, T., et al. (2014). PEGylated WS<sub>2</sub> nanosheets as a multifunctional theranostic agent for *in vivo* dual-modal CT/photoacoustic imaging guided photothermal therapy. *Adv. Mater.* 26, 1886–1893. doi: 10.1002/adma.201304497
- Chimene, D., Alge, D. L., and Gaharwar, A. K. (2015). Two-dimensional nanomaterials for biomedical applications: emerging trends and future prospects. *Adv. Mater.* 27, 7261–7284. doi: 10.1002/adma.201502422
- Choleva, T. G., Gatselou, V. A., Tsogas, G. Z., and Giokas, D. L. (2018). Intrinsic peroxidase-like activity of rhodium nanoparticles, and their application to the colorimetric determination of hydrogen peroxide and glucose. *Microchim. Acta* 185, 22–30. doi: 10.1007/s00604-017-2582-8
- Coleman, J. N., Lotya, M., O'Neill, A., Bergin, S. D., King, P. J., Khan, U., et al. (2011). Two-dimensional nanosheets produced by liquid exfoliation of layered materials. *Science* 331, 568–571. doi: 10.1126/science.1194975
- Darabdhara, G., Bordoloi, J., Manna, P., and Das, M. R. (2019). Biocompatible bimetallic Au-Ni doped graphitic carbon nitride sheets: a novel peroxidase-mimicking artificial enzyme for rapid and highly sensitive colorimetric detection of glucose. *Sens. Actuat. B* 285, 277–290. doi: 10.1016/j.snb.2019.01.048
- Ding, Y. J., Chen, Y. P., Zhang, X. L., Chen, L., Dong, Z. H., Jiang, H. L., et al. (2017). Controlled intercalation and chemical exfoliation of layered metal-organic frameworks using a chemically labile intercalating agent. *J. Am. Chem. Soc.* 139, 9136–9139. doi: 10.1021/jacs.7b04829
- Dong, Y. Q., Wang, Q., Wu, H. S., Chen, Y. M., Lu, C.-H., Chi, Y. W., et al. (2018). Graphitic carbon nitride materials: sensing, imaging and therapy. *Biomater. Sci.* 6, 2298–2311. doi: 10.1002/sml.201602056
- Duan, H. H., Yan, N., Yu, R., Chang, C. R., Zhou, G., Hu, H. S., et al. (2014). Ultrathin rhodium nanosheets. *Nat. Commun.* 5:3093. doi: 10.1038/ncomms4093
- Dutta, S., Ray, C., Mallick, S., Sarkar, S., Sahoo, R., Negishi, Y., et al. (2015). A gel-based approach to design hierarchical CuS decorated reduced graphene oxide nanosheets for enhanced peroxidase-like activity leading to colorimetric detection of dopamine. *J. Phys. Chem. C* 119, 23790–23800. doi: 10.1021/acs.jpcc.5b08421
- Feng, L. P., Zhang, L. X., Zhang, S., Chen, X., Li, P., Gao, Y., et al. (2020). Plasma-assisted controllable doping of nitrogen into MoS<sub>2</sub> nanosheets as efficient nanozymes with enhanced peroxidase-like catalysis activity. *ACS Appl. Mater. Interfaces* 12, 17547–17556. doi: 10.1021/acsmi.0c01789
- Gan, X. R., Zhao, H. M., and Quan, X. (2017). Two-dimensional MoS<sub>2</sub>: a promising building block for biosensors. *Biosens. Bioelectron.* 89, 56–71. doi: 10.1016/j.bios.2016.03.042
- Gao, F., Yang, X., Luo, X. P., Xue, X. L., Qian, C. G., and Sun, M. J. (2020). Photoactivated nanosheets accelerate nucleus access of cisplatin for drug-resistant cancer therapy. *Adv. Funct. Mater.* 2001546. doi: 10.1002/adfm.202001546
- Gao, L. Z., Zhuang, J., Nie, L., Zhang, J. B., Zhang, Y., Gu, N., et al. (2007). Intrinsic peroxidase-like activity of ferromagnetic nanoparticles. *Nat. Nanotechnol.* 2, 577–583. doi: 10.1038/nnano.2007.260
- Ge, J., Cai, R., Chen, X. G., Wu, Q., Zhang, L. L., Jiang, Y., et al. (2019). Facile approach to prepare HSA-templated MnO<sub>2</sub> nanosheets as oxidase mimic for colorimetric detection of glutathione. *Talanta* 195, 40–45. doi: 10.1016/j.talanta.2018.11.024
- Ghosal, K., and Sarkar, K. (2018). Biomedical applications of graphene nanomaterials and beyond. *ACS Biomater. Sci. Eng.* 4, 2653–2703. doi: 10.1021/acsbomaterials.8b00376
- Girish, C. M., Sasidharan, A., Gowd, G. S., Nair, S., and Koyakutty, M. (2013). Confocal Raman imaging study showing macrophage mediated biodegradation of graphene *in vivo*. *Adv. Healthcare Mater.* 2, 1489–1500. doi: 10.1002/adhm.201200489
- Gollavelli, G., and Ling, Y.-C. (2012). Multi-functional graphene as an *in vitro* and *in vivo* imaging probe. *Biomaterials* 33, 2532–2545. doi: 10.1016/j.biomaterials.2011.12.010
- Guan, G. J., and Han, M.-Y. (2019). Functionalized hybridization of 2D nanomaterials. *Adv. Sci.* 6:1901837. doi: 10.1002/advs.201901837

- Halim, A., Liu, L., Ariyanti, A. D., Ju, Y., Luo, Q., and Song, G. B. (2019). Low-dose suspended graphene oxide nanosheets induce antioxidant response and osteogenic differentiation of bone marrow-derived mesenchymal stem cells via JNK-dependent FoxO1 activation. *J. Mater. Chem. B*, 7, 5998–6009. doi: 10.1039/C9TB01413F
- Harvey, A., He, X. Y., Godwin, I. J., Backes, C., McAteer, D., Berner, N. C., et al. (2016). Production of Ni(OH)<sub>2</sub> nanosheets by liquid phase exfoliation: from optical properties to electrochemical applications. *J. Mater. Chem. A*, 4, 11046–11059. doi: 10.1039/C6TA02811J
- Hasan, M. A., Zaki, M. I., Pasupulety, L., and Kumari, K. (1999). Promotion of the hydrogen peroxide decomposition activity of manganese oxide catalysts. *Appl. Catal. A* 181:171. doi: 10.1016/S0926-860X(98)00430-X
- He, W., Jia, H., Li, X., Lei, Y., Li, J., Zhao, H., et al. (2012). Understanding the formation of CuS concave superstructures with peroxidase-like activity. *Nanoscale* 4, 3501–3506. doi: 10.1039/c2nr30310h
- He, W. W., Wu, X. C., Liu, J. B., Hu, X. N., Zhang, K., Hou, S., et al. (2010). Design of AgM bimetallic alloy nanostructures (M = Au, Pd, Pt) with tunable morphology and peroxidase-like activity. *Chem. Mater.* 22, 2988–2994. doi: 10.1021/cm100393v
- Heo, N. S., Song, H. P., Lee, S. M., Cho, H. J., Kim, H. J., Huh, Y. S., et al. (2020). Rosette-shaped graphitic carbon nitride acts as a peroxidase mimic in a wide pH range for fluorescence-based determination of glucose with glucose oxidase. *Microchim. Acta* 187:286. doi: 10.1007/s00604-020-04249-z
- Hu, T. T., Mei, X., Wang, Y. J., Weng, X. S., Liang, R. Z., and Wei, M. (2019). Two-dimensional nanomaterials: fascinating materials in biomedical field. *Sci. Bull.* 64, 1707–1727. doi: 10.1016/j.scib.2019.09.021
- Huang, J. K., Zhang, J. Z., Shi, G.-W., and Wei, Liu, Y. M. (2014). Hydrothermal synthesis of molybdenum disulfide nanosheets as supercapacitors electrode material. *Electrochim. Acta* 132, 397–403. doi: 10.1016/j.electacta.2014.04.007
- Huang, K., Li, Z. J., Lin, J., Han, G., and Huang, P. (2016). Two-dimensional transition metal carbides and nitrides (MXenes) for biomedical applications. *Chem. Soc. Rev.* 47, 5109–5124. *Small* 12, 5376–5393. doi: 10.1039/C7CS00838D
- Huang, L. J., Zhu, W. X., Zhang, W. T., Chen, K., Wang, J., Wang, R., et al. (2018). Layered Vanadium(IV) disulfide nanosheets as a peroxidase-like nanozyme for colorimetric detection of glucose. *Microchim. Acta* 185, 7–15. doi: 10.1007/s00604-017-2552-1
- Huang, X.-W., Wei, J. J., Liu, T., Zhang, X. L., Bai, S. M., and Yang, H. H. (2017). Silk fibroin-assisted exfoliation and functionalization of transition metal dichalcogenide nanosheets for antibacterial wound dressings. *Nanoscale* 9, 17193–17198. doi: 10.1039/C7NR06807G
- Huang, X. Q., Tang, S. H., Mu, X. L., Dai, Y., Chen, G. X., Zhou, Z. Y., et al. (2011). Freestanding palladium nanosheets with plasmonic and catalytic properties. *Nat. Nanotechnol.* 6, 28–32. doi: 10.1038/nnano.2010.235
- Huang, Y., Liu, C. Q., Pu, F., Liu, Z., Ren, J. S., and Qu, X. G. (2017b). A Go-Se nanocomposites as an antioxidant nanozyme for cytoprotection. *Chem. Commun.* 53, 3082–3085. doi: 10.1039/C7CC00045F
- Huang, Y., Zhao, M. T., Han, S. K., Lai, Z. C., Yang, J., Tan, C. L., et al. (2017a). Growth of Au nanoparticles on 2D metalloporphyrinic metal-organic framework nanosheets used as biomimetic catalysts for cascade reactions. *Adv. Mater.* 29:1700102. doi: 10.1002/adma.201700102
- Huang, Y. Y., Ren, J. S., and Qu, X. G. (2019). Nanozymes: classification, catalytic mechanisms, activity regulation, and applications. *Chem. Rev.* 119, 4357–4412. doi: 10.1021/acs.chemrev.8b00672
- Huo, C., Yan, Z., and Song, X. (2015). 2D materials via liquid exfoliation: a review on fabrication and applications. *Sci. Bull.* 60, 1994–2008. doi: 10.1007/s11434-015-0936-3
- Ivanova, M. N., Grayfer, E. D., Plotnikova, E. E., Kibis, L. S., Darabdhara, G., Boruah, P. K., et al. (2019). Pt-decorated boron nitride nanosheets as artificial nanozyme for detection of dopamine. *ACS Appl. Mater. Interfaces* 11, 22102–22112. doi: 10.1021/acsami.9b04144
- Jiang, C. M., Wu, C., Li, X. J., Yao, Y., Lan, L. Y., Zhao, F. N., et al. (2019). All-electrospun flexible triboelectric nanogenerator based on metallic MXene nanosheet. *Nano Energy* 59, 268–276. doi: 10.1016/j.nanoen.2019.02.052
- Jiang, D. W., Ni, D. L., Rosenkrans, Z. T., Huang, P., Yan, X. Y., and Cai, W. B. (2019). Nanozyme: new horizons for responsive biomedical applications. *Chem. Soc. Rev.* 48, 3683–3704. doi: 10.1039/C8CS00718G
- Jiao, L., Yan, H. Y., Wu, Y., Gu, W. L., Zhu, C. Z., Du, D., et al. (2019). When nanozymes meet single-atom catalysis. *Angew. Chem. Int. Ed.* 59, 2565–2576. doi: 10.1002/anie.201905645
- Ju, Y., and Kim, J. (2015). Dendrimer-encapsulated Pt nanoparticles with peroxidase-mimetic activity as biocatalytic labels for sensitive colorimetric analyses. *Chem. Commun.* 51, 13752–13755. doi: 10.1039/C5CC06055A
- Khan, K., Tareen, A. K., Aslam, M., Wang, R. H., Zhang, Y. P., Mahmood, A., et al. (2020). Recent developments in emerging two-dimensional materials and their applications. *J. Mater. Chem. C* 8, 387–440. doi: 10.1039/C9TC04187G
- Kim, M. S., Cho, S., Joo, S. H., Lee, J., Kwak, S. K., Kim, M. I., et al. (2019). N- and B-codoped graphene: a strong candidate to replace natural peroxidase in sensitive and selective bioassays. *ACS Nano* 13, 4312–4321. doi: 10.1021/acsnano.8b09519
- Kim, M. S., Lee, J., Kim, H. S., Cho, A., Shim, K. H., Le, T. N., et al. (2020). Heme cofactor-resembling Fe-N single site embedded graphene as nanozymes to selectively detect H<sub>2</sub>O<sub>2</sub> with high sensitivity. *Adv. Funct. Mater.* 30:1905410. doi: 10.1002/adfm.201905410
- Kong, L., Xing, L., Zhou, B., Du, L., and Shi, X. (2017). Dendrimer-modified MoS<sub>2</sub> nanoflakes as a platform for combinational gene silencing and photothermal therapy of tumors. *ACS Appl. Mater. Interfaces* 9, 15995–16005. doi: 10.1021/acscami.7b03371
- Korschelt, K., Ragg, R., Metzger, C. S., Kluncker, M., Oster, M., Barton, B., et al. (2017). Glycine-functionalized copper(II) hydroxide nanoparticles with high intrinsic superoxide dismutase activity. *Nanoscale* 9, 3952–3960. doi: 10.1039/C6NR09810J
- Korsvik, C., Patil, S., Seal, S., and Self, W. T. (2007). Superoxide dismutase mimetic properties exhibited by vacancy engineered ceria nanoparticles. *Chem. Commun.* 1056–1058. doi: 10.1039/b615134e
- Li, D., Muller, M. B., Gilje, S., Kaner, R. B., and Wallace, G. G. (2008). Processable aqueous dispersions of graphene nanosheets. *Nat. Nanotechnol.* 3, 101–105. doi: 10.1038/nnano.2007.451
- Li, Z. H., Liu, X. Y., Liang, X. H., Zhong, J. H., Guo, L. Q., and Fu, F. F. (2019). Colorimetric determination of xanthine in urine based on peroxidase-like activity of WO<sub>3</sub> nanosheets. *Talanta* 204, 278–284. doi: 10.1016/j.talanta.2019.06.003
- Liang, Q. H., Li, Z., Bai, Y., Huang, Z.-H., Kang, F. Y., and Yang, Q.-H. (2017). Reduced-sized monolayer carbon nitride nanosheets for highly improved photoresponse for cell imaging and photocatalysis. *Sci. China Mater.* 60, 109–118. doi: 10.1007/s40843-016-5131-9
- Liao, K.-H., Lin, Y.-S., Macosko, C. W., and Haynes, C. L. (2011). Cytotoxicity of graphene oxide and graphene in human erythrocytes and Skin Fibroblasts. *ACS Appl. Mater. Interfaces* 3, 2607–2615. doi: 10.1021/am200428v
- Lin, H., Wang, X. G., Yu, L. D., Chen, Y., and Shi, J. L. (2017). Two-dimensional ultrathin MXene ceramic nanosheets for photothermal conversion. *Nano Lett.* 17, 384–391. doi: 10.1021/acs.nanolett.6b04339
- Lin, S. S., and Gurol, M. D. (1998). Catalytic decomposition of hydrogen peroxide on iron oxide: kinetics, mechanism, and implication. *Environ. Sci. Technol.* 32, 1417–1423. doi: 10.1021/es970648k
- Lin, T. R., Zhong, L. S., Guo, L. Q., Fu, F. F., and Chen, G. N. (2014a). Seeing diabetes: visual detection of glucose based on the intrinsic peroxidase-like activity of MoS<sub>2</sub> nanosheets. *Nanoscale* 6, 11856–11862. doi: 10.1039/C4NR03393K
- Lin, T. R., Zhong, L. S., Song, Z. P., Guo, L. Q., Wu, H. Y., Guo, Q. Q., et al. (2014b). Visual detection of blood glucose based on peroxidase-like activity of WS<sub>2</sub> nanosheets. *Biosens. Bioelectron.* 62, 302–307. doi: 10.1016/j.bios.2014.07.001
- Lin, T. R., Zhong, L. S., Wang, J., Guo, L. Q., Wu, H. Y., Guo, Q. Q., et al. (2014c). Graphite-like carbon nitrides as peroxidase mimetics and their applications to glucose detection. *Biosens. Bioelectron.* 59, 89–93. doi: 10.1016/j.bios.2014.03.023
- Liu, J., Meng, L. J., Fei, Z. F., Dyson, P. J., Jing, X. N., and Liu, X. (2017). MnO<sub>2</sub> nanosheets as an artificial enzyme to mimic oxidase for rapid and sensitive detection of glutathione. *Biosens. Bioelectron.* 90, 69–74. doi: 10.1016/j.bios.2016.11.046
- Liu, J.-H., Yang, S.-T., Wang, H., Chang, Y., Cao, A., and Liu, Y. (2012). Effect of size and dose on the biodistribution of graphene oxide in mice. *Nanomedicine* 7, 1801–1812. doi: 10.2217/nmm.12.60
- Liu, T., Wang, C., Gu, X., Gong, H., Cheng, L., Shi, X. Z., et al. (2014). Drug delivery with PEGylated MoS<sub>2</sub> nano-sheets for combined

- photothermal and chemotherapy of cancer. *Adv. Mater.* 26, 3433–3440. doi: 10.1002/adma.201305256
- Liu, X. L., Wang, X. H., Han, Q. S., Qi, C., Wang, C., and Yang, R. (2019). Facile synthesis of IrO<sub>2</sub>/rGO nanocomposites with high peroxidase-like activity for sensitive colorimetric detection of low weight biothiols. *Talanta* 203, 227–234. doi: 10.1016/j.talanta.2019.05.070
- Liu, X. N., Huang, L. J., Wang, Y. P., Sun, J., Yue, T. L., Zhang, W. T., et al. (2020). One-pot bottom-up fabrication of a 2D/2D heterojunctioned nanozyme towards optimized peroxidase-like activity for sulfide ions sensing. *Sens. Actuat. B* 306:127565. doi: 10.1016/j.snb.2019.127565
- Liu, X. P., Yan, Z. Q., Zhang, Y., Liu, Z. W., Sun, Y. H., Ren, J. S., et al. (2019). Two-dimensional metal-organic framework/enzyme hybrid nanocatalyst as a benign and self-activated cascade reagent for *in vivo* wound healing. *ACS Nano* 13, 5222–5230. doi: 10.1021/acsnano.8b09501
- Liu, Y., Wu, H. H., Li, M., Yin, J.-J., and Nie, Z. H. (2014). pH dependent catalytic activities of platinum nanoparticles with respect to the decomposition of hydrogen peroxide and scavenging of superoxide and singlet oxygen. *Nanoscale* 6, 11904–11910. doi: 10.1039/C4NR03848G
- Lu, X. L., Feng, X. D., Werber, J. R., Chu, C. H., Zucker, I., Kim, J. H., et al. (2017). Enhanced antibacterial activity through the controlled alignment of graphene oxide nanosheets. *Proc. Natl. Acad. Sci. U. S. A.* 114, E9793–E9801. doi: 10.1073/pnas.1710996114
- Ma, D. Q., Xie, C. J., Wang, T., Mei, L. Q., Zhang, X., Guo, Z., et al. (2020). Liquid-phase exfoliation and functionalization of MoS<sub>2</sub> nanosheets for effective antibacterial application. *ChemBioChem* 21, 2373–2380. doi: 10.1002/cbic.202000195
- Ma, D. T., Zhao, J. L., Xie, J. L., Zhang, F., Wang, R., Wu, L. M., et al. (2020). Ultrathin boron nanosheets as an emerging two-dimensional photoluminescence material for bioimaging. *Nanoscale Horiz.* 5, 705–713. doi: 10.1039/C9NH00698B
- Maromeze, C. M., Dos Santos, G. P., De Moraes, V. B., Da, C. L., and Kubota, L. T. (2016). Multifunctional catalytic platform for peroxidase mimicking, enzyme immobilization and biosensing. *Biosens. Bioelectron.* 77, 746–751. doi: 10.1016/j.bios.2015.10.042
- Mateti, S., Wong, C. S., Liu, Z., Yang, W. R., Li, Y. C., Li, L. H., et al. (2018). Biocompatibility of boron nitride nanosheets. *Nano Res.* 11, 334–342. doi: 10.1007/s12274-017-1635-y
- Merlo, A., Mokkalapati, V. R. S. S., Pandit, S., and Mijakovic, I. (2018). Boron nitride nanomaterials: biocompatibility and bio-applications. *Biomater. Sci.* 6, 2298–2311. doi: 10.1039/C8BM00516H
- Mu, J. S., Wang, Y., Zhao, M., and Zhang, L. (2012). Intrinsic peroxidase-like activity and catalase-like activity of Co<sub>3</sub>O<sub>4</sub> nanoparticles. *Chem. Commun.* 48, 2540–2542. doi: 10.1039/c2cc17013b
- Mu, J. S., Zhang, L., Zhao, M., and Wang, Y. (2013). Co<sub>3</sub>O<sub>4</sub> nanoparticles as an efficient catalase mimic: properties, mechanism and its electrocatalytic sensing application for hydrogen peroxidase. *J. Mol. Catal. A Chem.* 378, 30–37. doi: 10.1016/j.molcata.2013.05.016
- Novoselov, K. S., Geim, A. K., Morozov, S. V., Jiang, D., Zhang, Y., Dubonos, S. V., et al. (2004). Electric field effect in atomically thin carbon films. *Science* 306, 666–669. doi: 10.1126/science.1102896
- Novoselov, K. S., Jiang, D., Schedin, F., Booth, T. J., Khotkevich, V. V., Morozov, S. V., et al. (2005). Two-dimensional atomic crystals. *Proc. Natl. Acad. Sci. U. S. A.* 102, 10451–10453. doi: 10.1073/pnas.0502848102
- Oudeng, G., Au, M., Shi, J., Wen, C., and Yang, M. (2018). One-step *in situ* detection of MiRNA-21 expression in single cancer cells based on biofunctionalized MoS<sub>2</sub> nanosheets. *ACS Appl. Mater. Interfaces* 10, 350–360. doi: 10.1021/acsmi.7b18102
- Ouyang, J., Deng, Y. Y., Chen, W. S., Xu, Q. F., Wang, L. Q., Liu, Z. J., et al. (2018). Marriage of artificial catalase and black phosphorous nanosheets for reinforced photodynamic antitumor therapy. *J. Mater. Chem. B* 6, 2057–2064. doi: 10.1039/C8TB00371H
- Qi, C., Cai, S. F., Wang, X. H., Li, J. Y., Lian, Z., Sun, S. S., et al. (2016). Enhanced oxidase/peroxidase-like activities of aptamer conjugated MoS<sub>2</sub>/PtCu nanocomposites and their biosensing application. *RSC Adv.* 6, 54949–54955. doi: 10.1039/C6RA03507H
- Qian, X., Gu, Z., and Chen, Y. (2017). Two-dimensional black phosphorus nanosheets for theranostic nanomedicine. *Mater. Horiz.* 4, 800–816. doi: 10.1039/C7MH00305F
- Ren, B. Y., Wang, Y. C., and Ou, J. Z. (2020). Engineering two-dimensional metal oxides via surface functionalization for biological applications. *J. Mater. Chem. B* 8, 1108–1127. doi: 10.1039/C9TB02423A
- Ren, X. Y., Huo, M. F., Wang, M. M., Lin, H., Zhang, X. X., Yin, J., et al. (2019). Highly catalytic niobium carbide (MXene) promotes hematopoietic recovery after radiation by free radical scavenging. *ACS Nano* 13, 6438–6454. doi: 10.1021/acsnano.8b09327
- Ruan, Y. D., Jia, X. D., Wang, C., Zhen, W. Y., and Jiang, X. E. (2018). Mn-Fe layered double hydroxide nanosheets: a new photothermal nanocarrier for O<sub>2</sub>-evolving phototherapy. *Chem. Commun.* 54, 11729–11732. doi: 10.1039/C8CC06033A
- Sasidharan, A., Panchakarla, L., Chandran, P., Menon, D., Nair, S., Rao, C., et al. (2011). Differential nano-bio interactions and toxicity effects of pristine versus functionalized graphene. *Nanoscale* 3, 2461–2464. doi: 10.1039/c1nr10172b
- Sasidharan, A., Panchakarla, L. S., Sadanandan, A. R., Ashokan, A., Chandran, P., Girish, C. M., et al. (2012). Hemocompatibility and macrophage response of pristine and functionalized graphene. *Small* 8, 1251–1263. doi: 10.1002/sml.201102393
- Shi, Y., Hamsen, C., Jia, X., Kim, K. K., Reina, A., Hofmann, M., et al. (2010). Synthesis of few-layer hexagonal boron nitride thin film by chemical vapor deposition. *Nano Lett.* 10, 4134–4139. doi: 10.1021/nl1023707
- Singh, S. K., Singh, M. K., Nayak, M. K., Kumari, S., Shrivastava, S., Grácio, J. J., et al. (2011). Thrombus inducing property of atomically thin graphene oxide sheets. *ACS Nano* 5, 4987–4996. doi: 10.1021/nn201092p
- Song, Y. J., Qu, K. G., Zhao, C., Ren, J. S., and Qu, X. G. (2010). Graphene oxide: intrinsic peroxidase catalytic activity and its application to glucose detection. *Adv. Mater.* 22, 2206–2210. doi: 10.1002/adma.200903783
- Song, Y. J., Wei, W. L., and Qu, X. G. (2011). Colorimetric biosensing using smart materials. *Adv. Mater.* 23, 4215–4236. doi: 10.1002/adma.201101853
- Su, L., Feng, J., Zhou, X. M., Ren, C. L., Li, H. H., and Chen, X. G. (2012). Colorimetric detection of urine glucose based ZnFe<sub>2</sub>O<sub>4</sub> magnetic-nanoparticles. *Anal. Chem.* 84, 5753–5758. doi: 10.1021/ac300939z
- Sukumar, T., Varghese, J., Suja Bhargavan, K. S., Jayasree, P., Suvakbala, V., Alaganandam, K., et al. (2020). Cytotoxicity of formulated graphene and its natural rubber nanocomposite thin film in human vaginal epithelial cells: an influence of noncovalent interaction. *ACS Biomater. Sci. Eng.* 6, 2007–2019. doi: 10.1021/acsbomaterials.9b01897
- Sun, H. Y., Liu, X. L., Wang, X. H., Han, Q. S., Qi, C., Li, Y. M., et al. (2020). Colorimetric determination of ascorbic acid using a polyallylamine-stabilized IrO<sub>2</sub>/graphene oxide nanozyme as a peroxidase mimic. *Microchim. Acta* 187:110. doi: 10.1007/s00604-019-3897-4
- Sun, X. M., Liu, Z., Welscher, K., Robinson, J. T., Goodwin, A., Zaric, S., et al. (2008). Nano-graphene oxide for cellular imaging and drug delivery. *Nano Res.* 1, 203–212. doi: 10.1007/s12274-008-8021-8
- Tan, C. L., Cao, X. H., Wu, X. J., He, Q. Y., Yang, J., Zhang, X., et al. (2017). Recent advances in ultrathin two-dimensional nanomaterials. *Chem. Rev.* 117, 6225–6331. doi: 10.1021/acs.chemrev.6b00558
- Tan, C. L., and Zhang, H. (2015). Wet-chemical synthesis and applications of non-layer structured two-dimensional nanomaterials. *Nat. Commun.* 6:7873. doi: 10.1038/ncomms8873
- Tang, Y., Hu, Y., Yang, Y. X., Liu, B. Y., and Wu, Y. G. (2020). A facile colorimetric sensor for ultrasensitive and selective detection of lead(II) in environmental and biological samples based on intrinsic peroxidase-mimic activity of WS<sub>2</sub> nanosheets. *Anal. Chim. Acta* 1106, 115–125. doi: 10.1016/j.aca.2020.01.043
- Tao, W., Kong, N., Ji, X. Y., Zhang, Y. P., Sharma, A., Ouyang, J., et al. (2019). Emerging two-dimensional monoelemental materials (Xenes) for biomedical applications. *Chem. Soc. Rev.* 48, 2891–2912. doi: 10.1039/C8CS00823J
- Tao, Y., Lin, Y. H., Huang, Z. Z., Ren, J. S., and Qu, X. G. (2013). Incorporating graphene oxide and gold nanoclusters: a synergistic catalyst with surprisingly high peroxidase-like activity over a broad pH range and its application for

- cancer cell detection. *Adv. Mater.* 25, 2594–2599. doi: 10.1002/adma.201204419
- Tian, J. Q., Liu, Q., Asiri, A. M., Qusti, A. H., Al-Youbi, A. O., and Sun, X. P. (2013). Ultrathin graphitic carbon nitride nanosheets: a novel peroxidase mimetic, Fe doping-mediated catalytic performance enhancement and application to rapid, highly sensitive optical detection of glucose. *Nanoscale* 5, 11604–11609. doi: 10.1039/c3nr03693f
- Vernekar, A. A., Sinha, D., Srivastava, S., Paramasivam, P. U., D'Silva, P., and Mughes, G. (2014). An antioxidant nanozyme that uncovers the cytoprotective potential of Vanadia nanowires. *Nat. Commun.* 5, 5301–5314. doi: 10.1038/ncomms6301
- Wang, J. Y., Li, W. Y., and Zheng, Y.-Q. (2019). Nitro-functionalized metal-organic frameworks with catalase mimic properties for glutathione detection. *Analyst* 144, 6041–6047. doi: 10.1039/C9AN00813F
- Wang, K., Ruan, J., Song, H., Zhang, J., Wo, Y., Guo, S., et al. (2011). Biocompatibility of graphene oxide. *Nanoscale Res. Lett.* 6:8. doi: 10.1007/s11671-010-9751-6
- Wang, S. G., Yang, X. Q., Zhou, L. L., Li, J. F., and Chen, H. R. (2020). 2D nanostructures beyond graphene: preparation, biocompatibility and biodegradation behaviors. *J. Mater. Chem. B* 8, 2974–2989. doi: 10.1039/C9TB02845E
- Wang, T., Zhang, X., Mei, L. Q., Ma, D. Q., Liao, Y., Zu, Y., et al. (2020). A two-step gas/liquid strategy for the production of N-doped defect-rich transition metal dichalcogenide nanosheets and their antibacterial applications. *Nanoscale* 12, 8415–8424. doi: 10.1039/D0NR00192A
- Wang, X. H., Han, Q. S., Cai, S. F., Wang, T., Yang, R., and Wang, C. (2017). Excellent peroxidase mimicking property of CuO/Pt nanocomposites and their application as an ascorbic acid sensor. *Analyst* 142, 2500–2506. doi: 10.1039/C7AN00589J
- Wang, Y., Hu, J., Zhuang, Q. F., and Ni, Y. N. (2016). Enhancing sensitivity and selectivity in a label-free colorimetric sensor for detection of iron(II) ions with luminescent molybdenum disulfide nanosheet-based peroxidase mimetics. *Biosens. Bioelectron.* 80, 111–117. doi: 10.1016/j.bios.2016.01.037
- Wang, Z. Z., Dong, K., Liu, Z., Zhang, Y., Chen, Z. W., Sun, H. J., et al. (2017). Activation of biologically relevant levels of reactive oxygen species by Au/g-C<sub>3</sub>N<sub>4</sub> hybrid nanozyme for bacteria killing and wound disinfection. *Biomaterials* 113, 145–157. doi: 10.1016/j.biomaterials.2016.10.041
- Wei, H., and Wang, E. K. (2013). Nanomaterials with enzyme-like characteristics (nanozymes): next-generation artificial enzymes. *Chem. Rev.* 42, 6060–6093. doi: 10.1039/c3cs35486e
- Wei, J. P., Chen, X. N., Shi, S. G., Mo, S. G., and Zheng, N. F. (2015). An investigation of the mimetic enzyme activity of two-dimensional Pd-based nanostructures. *Nanoscale* 7, 19018–19026. doi: 10.1039/C5NR05675F
- Wu, N., Wang, Y. T., Wang, X. N., Guo, F. N., Wen, H., and Yang, T. (2019). Enhanced peroxidase-like activity of Au NPs loaded graphitic carbon nitride nanosheets for colorimetric biosensing. *Anal. Chim. Acta* 1091, 69–75. doi: 10.1016/j.aca.2019.09.072
- Wu, X. J., Chen, T. M., Wang, J. X., and Yang, G. W. (2018). Few-layered MoSe<sub>2</sub> nanosheets as an efficient peroxidase nanozyme for highly sensitive colorimetric detection of H<sub>2</sub>O<sub>2</sub> and xanthine. *J. Mater. Chem. B* 6, 105–111. doi: 10.1039/C7TB02434G
- Wu, Z. N., Liu, J. L., Li, Y. C., Cheng, Z. Y., Li, T. T., Zhang, H., et al. (2015). Self-assembly of nanoclusters into mono-, few-, and multilayered sheets via dipole-induced asymmetric van der Waals attraction. *ACS Nano* 9, 6315–6323. doi: 10.1021/acsnano.5b01823
- Xuan, J. N., Wang, Z. Q., Chen, Y. Y., Liang, D. J., Cheng, L., Yang, X. J., et al. (2016). Organic-based-driven intercalation and delamination for the production of functionalized titanium carbide nanosheets with superior photothermal therapeutic performance. *Angew. Chem. Int. Ed.* 55, 14569–14574. doi: 10.1002/anie.201606643
- Yan, L., Gonca, S., Zhu, G. Y., Zhang, W. J., and Chen, X. F. (2019). Layered double hydroxide nanostructures and nanocomposites for biomedical applications. *J. Mater. Chem. B* 7, 5583–5601. doi: 10.1039/C9TB01312A
- Yan, X., Song, Y., Wu, X. L., Zhu, C. Z., Su, X. G., Du, D., et al. (2017). Oxidase-mimicking activity of ultrathin MnO<sub>2</sub> nanosheets in colorimetric assay of acetylcholinesterase activity. *Nanoscale* 9, 2317–2323. doi: 10.1039/C6NR08473G
- Yang, C., Feng, W. J., Li, Y., Tian, X. K., Zhou, Z. X., Lu, L. Q., et al. (2019). A promising method for diabetes early diagnosis via sensitive detection of urine glucose by Fe-Pd/rGO. *Dyes Pigments* 164, 20–26. doi: 10.1016/j.dyepig.2018.12.061
- Yang, H., Zhang, X., Tang, A., and Qiu, G. (2004). Gobalt ferrite nanoparticles prepared by coprecipitation/mechanicochemical treatment. *Chem. Lett.* 33, 826–827. doi: 10.1246/cl.2004.826
- Yang, S. B., Gong, Y. J., Zhang, J. S., Zhan, L., Ma, L. L., Fang, Z. Y., et al. (2013). Exfoliated graphitic carbon nitride nanosheets as efficient catalysts for hydrogen evolution under visible light. *Adv. Mater.* 25, 2452–2456. doi: 10.1002/adma.201204453
- Yang, W. N., Li, J., Yang, J., Liu, Y., Xu, Z. P., Sun, X. F., et al. (2020). Biomass-derived hierarchically porous CoFe-LDH/CeO<sub>2</sub> hybrid with peroxidase-like activity for colorimetric sensing of H<sub>2</sub>O<sub>2</sub> and glucose. *J. Alloy Compound* 815:152276. doi: 10.1016/j.jallcom.2019.152276
- Yi, M., and Shen, Z. (2015). A review on mechanical exfoliation for the scalable production of graphene. *J. Mater. Chem. A* 3, 11700–11715. doi: 10.1039/C5TA00252D
- Yim, D. B., Lee, D.-E., So, Y., Choi, C., Son, W., Jang, K., et al. (2020). Sustainable nanosheet antioxidants for sepsis therapy via scavenging intracellular reactive oxygen and nitrogen species. *ACS Nano* 14, 10324–10336. doi: 10.1021/acsnano.0c03807
- Yin, W. Y., Yan, L., Yu, J., Tian, G., Zhou, L. J., Zheng, X. P., et al. (2014). High-throughput synthesis of single-layer MoS<sub>2</sub> nanosheets as a near-infrared photothermal-triggered drug delivery for effective cancer therapy. *ACS Nano* 8, 6922–6933. doi: 10.1021/nn501647j
- Yong, Y., Zhou, L. J., Gu, Z. J., Yan, L., Tian, G., Zheng, X. P., et al. (2014). WS<sub>2</sub> nanosheet as a new photosensitizer carrier for combined photodynamic and photothermal therapy of cancer cells. *Nanoscale* 6, 10394–10403. doi: 10.1039/C4NR02453B
- Yu, F. T., Cangelosi, V. M., Zastrow, M. L., Tegoni, M., Plegaria, J. S., Tebo, A. G., Mocny, C. S., et al. (2014). Protein design: toward functional metalloenzymes. *Chem. Rev.* 114, 3495–3578. doi: 10.1021/cr400458x
- Yuwen, L., Yu, H., Yang, X., Zhou, J., Zhang, Q., Zhang, Y., et al. (2016). Rapid preparation of single-layer transition metal dichalcogenide nanosheets via ultrasonication enhanced lithium intercalation. *Chem. Commun.* 52, 529–532. doi: 10.1039/C5CC07301D
- Zeng, Z. Y., Yin, Z. Y., Huang, X., Li, H., He, Q. Y., Lu, G., et al. (2011). Single-layer semiconducting nanosheets: high-yield preparation and device fabrication. *Angew. Chem. Int. Ed.* 50, 11093–11097. doi: 10.1002/anie.201106004
- Zhan, T. R., Kang, J. X., Li, X. J., Pan, L., Li, G. J., and Hou, W. G. (2018). NiFe layered double hydroxide nanosheets as an efficiently mimic enzyme for colorimetric determination of glucose and H<sub>2</sub>O<sub>2</sub>. *Sens. Actuat. B* 255, 2635–2642. doi: 10.1016/j.snb.2017.09.074
- Zhang, H. (2015). Ultrathin two-dimensional nanomaterials. *ACS Nano* 9, 9451–9469. doi: 10.1021/acsnano.5b05040
- Zhang, L. N., Deng, H. H., Lin, F. L., Xu, X. W., Weng, S. H., Liu, A. L., et al. (2014). *In situ* growth of porous platinum nanoparticles on graphene oxide for colorimetric detection of cancer cells. *Anal. Chem.* 86, 2711–2718. doi: 10.1021/ac404104j
- Zhang, T., Lu, Y., Luo, G. (2014). Synthesis of hierarchical iron hydrogen phosphate crystal as a robust peroxidase mimic for stable H<sub>2</sub>O<sub>2</sub> detection. *ACS Appl. Mater. Interfaces* 6, 14433–14438. doi: 10.1021/am503708a
- Zhang, W. C., Li, X., Xu, X. C., He, Y. F., Qiu, F. X., Pan, J. M., et al. (2019). Pd nanoparticle-decorated graphitic C<sub>3</sub>N<sub>4</sub> nanosheets with bifunctional peroxidase mimicking and ON-OFF fluorescence enable naked-eye and fluorescent dual-readout sensing of glucose. *J. Mater. Chem. B* 7, 233–239. doi: 10.1039/C8TB02110D
- Zhang, X. L., Li, G. L., Wu, D., Li, X. L., Hu, N., Chen, J., et al. (2019). Recent progress in the design fabrication of metal-organic frameworks-based nanozymes and their applications to sensing and cancer



- therapy. *Biosens. Bioelectron.* 137, 178–198. doi: 10.1016/j.bios.2019.04.061
- Zhang, Y., Wang, Y. N., Sun, X. T., Chen, L., and Xu, Z. R. (2017). Boron nitride nanosheet/CuS nanocomposites as mimetic peroxidase for sensitive colorimetric detection of cholesterol. *Sens. Actuat. B* 246, 118–126. doi: 10.1016/j.snb.2017.02.059
- Zhou, X. F., Zheng, X. L., Yan, B., Xu, T., and Xu, Q. (2017). Defect engineering of two-dimensional WO<sub>3</sub> nanosheets for enhanced electrochromism and photoelectrochemical performance. *Appl. Surf. Sci.* 400, 57–63. doi: 10.1016/j.apsusc.2016.12.072
- Zhu, C. F., Zeng, Z. Y., Li, H., Li, F., Fan, C. H., and Zhang, H. (2013). Single-layer MoS<sub>2</sub>-based nanoprobe for homogeneous detection of biomolecules. *J. Am. Chem. Soc.* 135, 5998–6001. doi: 10.1021/ja4019572

**Conflict of Interest:** The authors declare that the research was conducted in the absence of any commercial or financial relationships that could be construed as a potential conflict of interest.

The handling Editor declared a shared affiliation, though no other collaboration, with one of the authors SC and RY.

*Copyright © 2020 Cai and Yang. This is an open-access article distributed under the terms of the Creative Commons Attribution License (CC BY). The use, distribution or reproduction in other forums is permitted, provided the original author(s) and the copyright owner(s) are credited and that the original publication in this journal is cited, in accordance with accepted academic practice. No use, distribution or reproduction is permitted which does not comply with these terms.*